Hurst phenomenon and fractional Gaussian noise made easy

Demetris Koutsoyiannis

Department of Water Resources, Faculty of Civil Engineering, National Technical University, Athens, Heroon Polytechneiou 5, GR-157 80 Zographou, Greece

(dk@hydro.ntua.gr)

Abstract. The Hurst phenomenon, which characterises hydrological and other geophysical time series, is formulated and studied in an easy manner in terms of the variance and autocorrelation of a stochastic process on multiple temporal scales. In addition, a simple explanation of the Hurst phenomenon based on the fluctuation of a hydrologic process upon different temporal scales is presented. The stochastic process that was devised to represent the Hurst phenomenon, i.e. the fractional Gaussian noise, is also studied on the same grounds. Based on its studied properties, three simple and fast methods to generate fractional Gaussian noise or good approximations of it are proposed.

Keywords. Hurst phenomenon; Fractional Gaussian noise; Persistence; Climate change.

Le phénomène Hurst et le bruit fractionnel gaussien rendus faciles dans leur utilisation

Résumé. On formule et étudie d'une manière simple le phénomène Hurst, qui caractérise les séries chronologiques en hydrologie et en géophysique, en termes de la variance et de l` autocorrélation d`un processus stochastique considéré dans des échelles temporelles multiples. De plus, on présente une explication simple du phénomène Hurst sur la base de la fluctuation d`un processus hydrologique dans des échelles temporelles multiples. On étudie aussi d'une manière analogue le bruit fractionnel gaussien qui constitue le processus stochastique construit pour représenter le phénomène Hurst. Se basant sur les propriétés étudiées de ce processus, on propose trois méthodes simples et rapides qui permettent de générer du bruit fractionnel gaussien ou de bonnes approximations de ceci.

Mots clefs. Phénomène Hurst; Bruit fractionnel gaussien; Persistance; Changement climatique.

1. Introduction

While investigating the discharge time series of the Nile River in the framework of the design of the Aswan High Dam, E. H. Hurst (1951) discovered a special behaviour of hydrologic and other geophysical time series, which has become known as the 'Hurst phenomenon'. This behaviour is essentially the tendency of wet years to cluster into wet periods or of dry years to cluster into drought periods. The term 'Joseph effect' introduced by Mandelbrot (1977, p. 248) has been used as an alternative for the same behaviour. Since its original discovery, the Hurst phenomenon has been verified in several environmental quantities such as wind power variations (Haslet and Raftery, 1989); global mean temperatures (Bloomfield, 1992); flows of the river Nile (Eltahir, 1996); flows of the river Warta, Poland (Radziejewski and Kundzewicz, 1997); monthly and daily inflows of Lake Maggiore, Italy (Montanari et al., 1997); annual streamflow records across the continental United States (Vogel et al., 1998); and indexes of North Atlantic Oscillation (Stephenson et al., 2000). In addition, the Hurst phenomenon has gained new interest today due to its relation to climate changes (e.g. Evans, 1996).

Hurst (1951) formulated mathematically his discovery in terms of the so-called rescaled range, which is a storage-related feature of a time series (Salas, 1993, p. 19.14; see also Appendix A1). Several types of models such as fractional Gaussian noise (FGN) models (Mandelbrot, 1965; Mandelbrot and Wallis, 1969a, b, c), fast fractional Gaussian noise models (Mandelbrot, 1971), broken line models (Ditlevsen, 1971; Mejia et al., 1972), fractional autoregressive integrated moving-average models (Hosking, 1981, 1984), and symmetric moving average models based on a generalised autocovariance structure (Koutsoyiannis, 2000) have been proposed to reproduce the Hurst phenomenon when generating synthetic time series (see also Bras and Rodriguez-Iturbe, 1985, pp. 210-280).

Although hydrologists may agree that the Hurst phenomenon is inherent to hydrologic time series, generally they prefer to use other, more convenient models to generate synthetic hydrologic time series, such as autoregressive (AR) models, moving average (MA) models, or combinations of the two (ARMA). For example, widespread stochastic hydrology packages

such as LAST (Lane and Frevert, 1990), SPIGOT (Grygier and Stedinger, 1990), and CSUPAC1 (Salas, 1993) have not implemented any of the above listed types of models that respect the Hurst phenomenon but rather they use AR, MA and ARMA models, which, however, cannot reproduce the Hurst phenomenon. It is also known that this reproduction may be essential in reservoir studies, especially in reservoirs performing overyear regulation with draft close to the mean annual inflow (Bras and Rodriguez-Iturbe, 1985, p. 265).

There must be several reasons explaining this unwillingness to reproduce the Hurst phenomenon in hydrologic practice. First, it is difficult to understand and explain, at least in comparison to typical statistical behaviour of everyday life processes. Stochastic hydrology texts (e.g. Yevjevich, 1972, pp. 131-172; Haan, 1977, p. 310; Kottegoda, 1980, pp. 184-203; Bras and Rodriguez-Iturbe, 1985, pp. 210-265; Salas et al., 1988, p. 240; Salas, 1993) adopt the original Hurst's approach, which is in terms of range analysis of hydrologic series; as it is shown in Appendix A1, the range analysis involves complexity and estimation problems. In addition, the nature of the Hurst phenomenon has been the subject of debate, as discussed by Bras and Rodriguez-Iturbe (1985, p. 214). Second, the algorithms that are used to generate synthetic data series respecting the Hurst phenomenon are complicated. Third, the typical models of this category have several weak points such as narrow type of autocorrelation functions that they can preserve, and difficulties to preserve skewness and to perform in multivariate problems.

Contrary to these, in this paper we attempt to show that the Hurst phenomenon is essentially very simple to formulate, understand and reproduce in synthetic series – in some aspects much simpler than the typical AR processes (some aspects of which are examined in section 2), which, in addition, are not consistent with long historical hydroclimatic records (section 3). We offer a mathematical formulation based on the relationship of the process variance with the temporal scale of the process (section 4). In addition, we attempt to offer a simple explanation of the Hurst phenomenon based on the fluctuation of a hydrologic process upon different timescales (section 5). We also provide three simple methods to generate fractional Gaussian noise or good approximations of it (section 6). Some mathematical derivations are given in Appendix A2. Throughout this paper, we totally avoid using the range

concept and range analysis. To explain the reasons why we avoid the range concept and also to link this presentation with the existing approaches of the Hurst phenomenon, we include Appendix A1, which is devoted to range related topics.

Throughout the paper, the presentation of all issues is made as simple as possible; this is done intentionally because the purpose of the paper is *not* to review the state of the art of the research related to the Hurst phenomenon, *nor* to give the complete mathematical details of it (for the latter see the comprehensive monograph by Beran, 1994) but rather (a) to assemble an easy to understand mathematical basis and physical explanation of the phenomenon and (b) to provide means for an easy implementation (e.g. using a spreadsheet package) of the methods, both for estimation and simulation. To this aim, some original simple algorithms are provided.

2. Multiple timescale properties of typical stochastic processes

Hydrologic processes such as rainfall, runoff, evaporation, etc., are often modelled as stationary stochastic processes in discrete time. Let us denote such a process X_i with $i = 1, 2, \ldots$, denoting discrete time (e.g. years). Further, let us denote its mean $\mu := E[X_i]$, its autocovariance $\gamma_j := \mathrm{Cov}[X_i, X_{i+j}]$ and its autocorrelation $\rho_j := \mathrm{Corr}[X_i, X_{i+j}] = \gamma_j / \gamma_0$ ($j = 0, \pm1, \pm2, \ldots$).

If fact, the time i represents the continuous time interval $[(i-1)\delta, i\,\delta)$ where δ is the timescale of interest. Very often, there is not a single scale of interest but many of them, which are integer multiples of a basic timescale δ. For example, when investigating the firm yield of a reservoir that performs overyear regulation, the basic timescale could be one year but timescales of several years are also of interest. Similarly, in short-scale rainfall modelling the basic timescale could be 5 or 10 minutes, but timescales of several hours are of interest, too. Let $k\,\delta$ be a timescale larger than the basic timescale δ where k is a positive integer (for convenience we will omit δ and speak about timescale k). We denote $Z_i^{(k)}$ the aggregated stochastic process on that timescale, i.e.,

$$Z_i^{(k)} := \sum_{l=(i-1)\,k+1}^{i\,k} X_l \tag{1}$$

Obviously, for $k = 1$, $Z_i^{(1)} \equiv X_i$; for $k = 2$, $Z_1^{(2)} := X_1 + X_2$, $Z_2^{(2)} := X_3 + X_4$; for $k = 3$, $Z_1^{(3)} := X_1 + X_2 + X_3$, $Z_2^{(3)} := X_4 + X_5 + X_6$, etc. The statistical characteristics of $Z_i^{(k)}$ for any timescale k can be derived from those of X_i. For example, the mean is

$$E[Z_i^{(k)}] = k\,\mu \tag{2}$$

whilst the variance and autocovariance (or autocorrelation) is more difficult to derive as it depends on the specific structure of γ_j (or ρ_j). A general expression that gives the covariance at any scale k in terms of that at the basic scale can be found using (1); this is

$$\gamma_j^{(k)} := \mathrm{Cov}[Z_i^{(k)}, Z_{i+j}^{(k)}] = \sum_{l=1}^{k} \sum_{m=j\,k+1}^{(j+1)\,k} \gamma_{m-l}, \qquad j = 0, \pm 1, \pm 2, \ldots \tag{3}$$

The autocovariance is related to the power spectrum of the process, which in general case is the discrete Fourier transform (DFT; also termed the inverse finite Fourier transform) of γ_j (e.g., Papoulis, 1991, pp. 118, 333; Bloomfield, 1976, pp. 46-49; Debnath, 1995, pp. 265-266), that is

$$s_\gamma^{(k)}(\omega) := 2\,\gamma_0^{(k)} + 4 \sum_{j=1}^{\infty} \gamma_j^{(k)} \cos(2\pi j\,\omega) = 2 \sum_{j=-\infty}^{\infty} \gamma_j^{(k)} \cos(2\pi j\,\omega) \tag{4}$$

Because γ_j is an even function of j (i.e., $\gamma_j = \gamma_{-j}$), the DFT in (4) is a cosine transform; as usually we have assumed in (4) that the frequency ω ranges in [0, 1/2], so that γ_j is determined in terms of $s_\gamma(\omega)$ by the finite Fourier transform

$$\gamma_j^{(k)} = \int_0^{1/2} s_\gamma^{(k)}(\omega) \cos(2\pi j\,\omega)\, d\omega \tag{5}$$

Before we study the process known as fractional Gaussian noise (FGN), which respects the Hurst phenomenon (this will be done in section 4), it may be a good idea to refer to two of the simplest stochastic models that we are more familiar with.

The first is white the noise, in which different X_i are independent identically distributed random variables, so that $\gamma_j = 0$ (and $\rho_j = 0$) for $j \neq 0$. Apparently then, the aggregated process will have variance

$$\gamma_0^{(k)} := \mathrm{Var}[Z_i^{(k)}] = k\,\gamma_0 \tag{6}$$

autocovariance $\gamma_j^{(k)} = 0$ and autocorrelation $\rho_j^{(k)} = 0$. From (4) we easily find that its power spectrum is constant, independent of the frequency ω, i.e.,

$$s_\gamma^{(k)}(\omega) / \gamma_0^{(k)} = 2 \tag{7}$$

In fact, the constant value of the power spectrum, i.e., the presence of all frequencies ω with the same magnitude, has been the reason for the term 'white noise'.

As a second example, let us assume that the process X_i at the basic timescale is the simpler possible process with some dependence of the current value on previous ones, also termed memory of the process. This is the autoregressive process of order 1 (AR(1)) and the dependence is expressed by

$$X_i = \rho\, X_{i-1} + V_i \tag{8}$$

where ρ is the lag one autocorrelation coefficient ($-1 < \rho < 1$) and V_i ($i = 1, 2, \ldots$) are innovations, i.e. independent identically distributed random variables with mean $(1-\rho)\,\mu$ and variance $(1-\rho^2)\,\gamma_0$. The process is also termed Markovian because the dependence of the current variable X_i on the previous variable X_{i-1} suffices to express completely the dependence of the present on the past. The autocorrelation of X_i is

$$\rho_j := \mathrm{Corr}[X_i, X_{i+j}] = \rho^{|j|} \tag{9}$$

Combining (9) and (3) after some algebra we find for the aggregated process

$$\gamma_0^{(k)} = \gamma_0 \frac{k\,(1-\rho^2) - 2\rho\,(1-\rho^k)}{(1-\rho)^2} \tag{10}$$

$$\gamma_j^{(k)} = \gamma_0 \frac{\rho^{kj-k+1}\,(1-\rho^k)^2}{(1-\rho)^2}, \quad j \geq 1 \tag{11}$$

and thus the autocorrelation is

$$\rho_j^{(k)} = \rho_1^{(k)} \rho^{k(j-1)}, \quad j \geq 1 \tag{12}$$

with

$$\rho_1^{(k)} = \frac{\rho\,(1-\rho^k)^2}{k\,(1-\rho^2) - 2\rho\,(1-\rho^k)} \tag{13}$$

By comparing (12)-(13) with (9) we conclude that $Z_i^{(k)}$ is no longer a Markovian process but a more complicated one (in fact (12) corresponds to an ARMA(1, 1) process; Box et al., 1994, p. 81). In other words, the simple AR(1) process is an AR(1) process only on its basic timescale, whereas it becomes more complicated on aggregated timescales.

The power spectrum of the aggregated process $Z_i^{(k)}$ can be found by adapting the power spectrum of the AR(1) process (Box et al., 1994, p. 58). After algebraic manipulations we get

$$s_\gamma^{(k)}(\omega) / \gamma_0^{(k)} = 2 + 4\,\rho_1^{(k)} \frac{\cos(2\pi\omega) - \rho^k}{1 + \rho^{2k} - 2\,\rho^k \cos(2\pi\omega)} \tag{14}$$

For relatively small k, this gives a characteristic inverse S-shaped power spectrum that corresponds to a short memory process.

For a large aggregated timescale k, the numerator of (10) is dominated by the first term and the variance of the aggregated process becomes

$$\gamma_0^{(k)} \approx k \frac{1+\rho}{1-\rho} \gamma_0 \tag{15}$$

i.e., it becomes proportional to the timescale k, similarly as in the white noise process. Also, from (13) we observe that $\rho_1^{(k)}$ becomes small, as does $\rho_j^{(k)}$. Consequently, from (14) we conclude that the power spectrum becomes $s_\gamma(\omega) / \gamma_0 = 2$, which characterises white noise.

In conclusion, if the process of interest is Markovian at the basic timescale, it tends to white noise for progressively increasing timescales. (In fact this happens with higher order AR and ARMA processes as well).

3. Some real world examples

Empirical evidence suggests that long historical hydroclimatic series may exhibit a behaviour very different from that implied by simple models such as the above described, or even more complicated models such as the ARMA ones. To demonstrate this we use two real world examples. The first is the most intensively studied series, which also led to the discovery of the Hurst phenomenon (Hurst, 1951): the series of the annual minimum water level of the Nile river for the years 622 to 1284 A.D. (663 observations), measured at the Roda Nilometer near Cairo (Toussoun, 1925, p. 366-385; Beran, 1994). The data is available from http://lib.stat.cmu.edu/S/beran. The second example is an even longer record; the series of standardised tree ring widths from a paleoclimatology study at Mammoth Creek, Utah, for the years 0-1989 (1990 values; Year 0 in fact stands for 1 B.C. as the calendar does not contain Year 0). The data, originated from pine trees at elevation 2590 m, latitude 37:39, longitude 112:40 (Graybill, 1990) is available from ftp://ftp.ngdc.noaa.gov/paleo/treering/chronologies/asciifiles/usawest/ut509.crn.

In Figure 1 we have plotted the data values versus time for both example data sets. In addition, we have plotted the 5-year and 25-year averages, which represent the aggregated processes at timescales k = 5 and 25, respectively. For comparison we have also plotted a series of white noise with statistics same to those of standardised tree rings. We can observe that fluctuations of the aggregated processes, especially for k = 25, are much greater in the real world time series than in the white noise series. These fluctuations could be taken as nonstationarities, that is, deterministic rising or falling trends that last 100-200 or more years. For example, if one had available only the data of the period 700-800 of either of the two time series, he or she would speak about a deterministic falling trend; similarly, one would speak about a regular rising trend of the Nile level between the years 1000-1100 or of the Utah series between years 100-300. However, the complete pictures for both series suggest that these trends are parts of large-scale random fluctuations rather than deterministic trends.

In Figure 2 we have plotted on logarithmic diagrams the standard deviation of the aggregated processes versus timescale k for the two example data sets. For comparison we

have also plotted theoretical curves for the white noise and AR(1) models (equations (6) and (10), respectively). Clearly, the plots of both series are almost straight lines on the logarithmic diagram with slopes 0.75-0.85. Both the white noise and the AR(1) models result in a slope equal to 0.5, significantly departing from historical data.

Furthermore, in Figure 3 we have plotted the autocorrelation coefficients of the aggregated processes for lag one and lag two, versus the timescale k, for the two example data sets. For comparison we have also plotted theoretical curves for the AR(1) model. The empirical autocorrelation coefficients are almost constant for all timescales whereas the AR(1) model results in autocorrelations that drop down to zero for large timescales.

Finally, in Figure 4 we have plotted the autocorrelation functions of the two example time series at the basic (annual) timescale along with the theoretical curves of the AR(1) model. Clearly, the curves of the AR(1) vanish off for lags 4-10 whereas the curves of the historical series are fat tailed and do not vanish for lags as high as 50. In conclusion, this discussion provides some further evidence, using a multiple-timescale approach, to the well-known fact that the AR(1) model is inconsistent with hydroclimatic reality (a similar conclusion can be drawn for more complex processes of the ARMA type).

4. The fractional Gaussian noise process

To restore consistency with reality, Mandelbrot (1965) introduced the process known as fractional Gaussian noise (FGN). The FGN process can be defined in discrete time (which is our scope here) in a manner similar to that used in continuous time (e.g. Saupe, 1988, p. 82; Abry et al., 1995). Specifically, the FGN process can be defined as a process satisfying the condition

$$(Z_i^{(k)} - k\,\mu) \overset{\mathrm{d}}{=} \left(\frac{k}{l}\right)^{H} (Z_j^{(l)} - l\,\mu) \tag{16}$$

where the symbol $\overset{\mathrm{d}}{=}$ stands for equality in (finite dimensional joint) distribution and H is a positive constant ($0 < H < 1$) known as the Hurst exponent (or coefficient). Equation (16) is

valid for any integer i and j (that is, the process is stationary) and any timescales k and l. As a consequence, for $i = j = l = 1$ we get

$$\gamma_0^{(k)} := \mathrm{Var}[Z_i^{(k)}] = k^{2H}\,\gamma_0 \tag{17}$$

Thus, the standard deviation is a power law of k with exponent H, which agrees with the observation on the real world cases of section 3. The extremely simple relation (17) can serve as the basis for estimating H (Montanari et al., 1997).

It is easy then to show (see Appendix A2) that, for any aggregated timescale k, the autocovariance function is independent of k, again agreeing with the observation of section 3. Specifically, it is given by

$$\rho_j^{(k)} = \rho_j = (1/2)\,[(j+1)^{2H} + (j-1)^{2H}] - j^{2H}, \qquad j > 0 \tag{18}$$

Apart from small j, this function is very well approximated by

$$\rho_j^{(k)} = \rho_j = H\,(2H-1)\,j^{2H-2} \tag{19}$$

which shows that autocorrelation is a power function of lag.

Notably, (18) can be obtained from a continuous time process $\Xi(t)$ with autocorrelation $\mathrm{Cov}[\Xi(t), \Xi(t+\tau)] = a\,\tau^{2H-2}$ (with constant $a = H\,(2H-1)\,\gamma_0$), by discretising the process using time intervals of any length δ and taking as X_i the average of $\Xi(t)$ in the interval $[i\,\delta, (i+1)\,\delta]$. This enables an approximate calculation of the power spectrum of the process as

$$s_\gamma^{(k)}(\omega) = 2\sum_{j=-\infty}^{\infty}\gamma_j^{(k)}\cos(2\pi j\omega) \approx 4\int_0^{\infty} a\,\tau^{2H-2}\cos(2\pi\tau\omega)\,d\tau \tag{20}$$

which results in the approximation $s_\gamma^{(k)}(\omega) \approx a'\,\omega^{1-2H}$. To find the constant a' so as to preserve exactly the process variance γ_0 we use (5) to get

$$\gamma_0^{(k)} = \int_0^{1/2} a'\,\omega^{1-2H}\,d\omega = \frac{a'}{(2-2H)\,2^{2-2H}} \tag{21}$$

from which we finally obtain

$$s_{\gamma}^{(k)}(\omega) / \gamma_0^{(k)} \approx 4\,(1-H)\,(2\,\omega)^{1-2H} \qquad (22)$$

which is a power law of the frequency ω.

Similarly to the AR(1) process, which uses one single parameter ρ to express the correlation structure of the process, the FGN process uses again one parameter, the Hurst exponent H. Therefore we can characterise the FGN process as a simplified model of reality, noting that it is much more effective in representing hydroclimatic series than the AR(1) process. A generalised and comprehensive family of processes, which can have a larger number of parameters and incorporates both the FGN and the ARMA processes, has been introduced by Koutsoyiannis (2000).

Comparing the FGN process to the AR(1) process in terms of the expressions of the basic statistical properties at multiple timescales, we observe that the former is rather simpler than the latter. Thus, the expression of the process variance at any scale k (equation (17)) is much simpler that that of AR(1) (equation (10)). Similarly, the expression of the process correlation at any scale k (equation (18))) is simpler that that of AR(1) (equations (12) and (13)).

5. A physical explanation

We are very familiar with a white noise process, a process where each event is totally independent from previous ones, e.g., a sequence of outcomes of consecutive throws of dice. Under the assumption of a stable climate, the maximum flood peaks of consecutive years form a white noise process, as well, as there is no stochastic dependence between flood events belonging to different hydrologic years. We are less familiar with processes that have some memory, but we can understand Markovian (e.g., AR(1)) processes. For example, Yevjevich (1972, p. 27) explained that the annual flow series is dependent and follows a Markovian process. To show this, Yevjevich assumed that the catchment is stimulated by an effective precipitation process that is white noise and that the water carry-over from year to year is ruled by a groundwater recession curve that is an exponential function of time.

However, the Hurst phenomenon and the related FGN process are more difficult to understand. Mesa and Poveda (1993) classify the Hurst phenomenon as one of the most

important unsolved problems in hydrology and state that "something quite dramatic must be happening from a physical point of view". The FGN process is very different from a Markovian process in that it implies a fat tailed autocorrelation function. For instance, if the Hurst coefficient is 0.85, as in the Nile example given in section 3, then the autocorrelation for lag 100 (years) is as high as 0.15, whereas if the process were Markovian the autocorrelation would be practically zero even for lags 10 times less. Does the explanation of this behaviour of natural systems, such as Nile's water level or Mammoth Creek's tree ring widths, rest on the self-organised criticality principle (Bak, 1996, pp. 21, 22, 31, 37), i.e., a cooperative behaviour, where the different items of large systems act together in some concerted way? Or, is it rest on monotonic deterministic trends (Bhattachara et al., 1983), which can explain mathematically this behaviour? Or, is there any natural mechanism inducing a long memory to the system, which is responsible for the high autocorrelation for a lag of 100 years or more?

The author's explanation is much simpler and relies upon an 'absence of memory' concept rather than a 'long-term memory' concept. That is, we set the hypothesis that not only does the system 'disremember' what was the value of the process 100 years (or more) ago, but it further 'forgets' what the process mean at that time was. This explanation is consistence with the assertion of the National Research Council (1991, p. 21) that climate "changes irregularly, for unknown reasons, on all timescales". The idea of irregular sporadic changes in the mean of the process appeared also in Salas and Boes (1980), but not in connection with FGN and not in the setting of multiple timescales. The idea of composite random processes with two timescales of fluctuation appeared in Vanmarcke (1983, p. 225). For more mathematical explanations of FGN the interested reader is referenced to Beran (1994, pp. 14-20).

To demonstrate our explanation let us start with a (easy to understand) Markovian process U_i, like the one graphically demonstrated in Figure 5(a), with mean $\mu := E[U_i]$, variance γ_0 and lag one autocorrelation coefficient $\rho = 0.20$. The autocorrelation function (given by (9)) for lags up to 1000 is shown in Figure 6(a) along with the autocorrelation function for the FGN process with same lag one autocorrelation coefficient (0.20). We observe the large difference

of the two autocorrelation functions: that of the Markovian process practically vanishes off at lag 4 whereas that of the FGN process has positive values for lags as high as 100.

Now, let as construct a second process V_i by subtracting from the process U_i its mean $E[U_i] = \mu$ and superimposing the result to a new random process M that has again mean μ and some variance Var[M] (see explanatory sketch on Figure 5(b)). From a practical point of view, V_i could be considered similar to U_i but with time varying mean M. For the latter we assume that (a) any realisation m of M lasts a number of years N and is independent from previous realisations; (b) N is a random variable exponentially distributed with mean λ. (This means that N can take non-integer values, which is not a problem). In other words, M takes a value $m_{(1)}$ that lasts n_1 years, then it changes to a value $m_{(2)}$ that lasts n_2 years, etc (where the values $m_{(1)}$, $m_{(2)}$, … can be generated from any distribution). The exponential distribution of N indicates that the points of change are random points in time (Papoulis, 1991, p. 57). If we denote M_i the instance of the M process at time i, it can be shown that M_i is also Markovian with lag one autocorrelation $\varphi := e^{-1/\lambda}$ (the proof is omitted). The process V_i can be expressed in terms of U_i and M_i as

$$V_i = U_i + M_i - \mu \tag{23}$$

For a conceptualisation of V_i let as consider the simpler case that M_i is a deterministic component, rather than a random process, with known value m_i at any time i, in which case $V_i = U_i + m_i - \mu$. Then V_i would be identical in distribution with U_i except that its mean would be $E[U_i] + m_i - \mu = m_i$ rather than μ. That is, V_i would be nonstationary with a time varying mean m_i (and all other moments constant in time). Returning back to our initial assumption that M_i is a random process, we infer from (23) that, since V_i is the sum of two stationary processes (U_i and M_i), it is a stationary process itself with mean μ.

It can be easily shown from (23) that the autocorrelation of V_i for lag j is

$$\mathrm{Corr}[V_i, V_{i+j}] = (1 - c)\rho^j + c\,\varphi^j \tag{24}$$

where c := Var[M_i] / (Var[M_i] + Var[U_i]). Setting for instance λ = 7.5 years and c = 0. 146 we get the autocorrelation function shown in Figure 6(b), which has departed from the AR(1) autocorrelation and approached the FGN autocorrelation.

Further, let us take another step to construct a third process W_i by subtracting from the process V_i its mean $E[V_i] = \mu$ and superimposing the result to a new random process P that has again mean μ (see explanatory sketch on Figure 5(c)). For the latter we make similar assumptions as in the previous step denoting by v the mean time between changes of the value of P and setting $\xi := e^{-1/v}$. The resulting composite process will be

$$W_i = V_i + P_i - \mu = U_i + M_i + P_i - 2\,\mu \tag{25}$$

Working as in the previous step we find

$$\text{Corr}[W_i, W_{i+j}] = (1 - c_1 - c_2)\rho^j + c_1\,\varphi^j + c_2\,\xi^j \tag{26}$$

where c_1 and c_2 are positive constants (with $c_1 + c_2 < 1$). Setting for instance λ = 7.5 years, v = 200 years, c_1 = 0.146 and c_2 = 0.036 we get the autocorrelation function shown in Figure 6(c), which has now become almost indistinguishable from the FGN autocorrelation for time lags from 1 to 1000.

This example illustrated that a Markovian underlying process can result in a nearly FGN process if there occur random fluctuations of the mean of a process at two different scales (e.g., 7.5 and 200 years), yet the resulting composite process being stationary. If we consider that fluctuations occur at a greater number of timescales, the degree of approximation of the composite process to the FGN process will be even better and can cover time lags greater than 1000 (although the extension to lags beyond 1000 may not have any practical interest in hydrology). In conclusion, the *irregular* changes of climate that, according to National Research Council (1991, p. 21), occur on all time scales can be responsible for, and explain, the Hurst phenomenon.

In the above example we considered that the process U, which represents the random fluctuations at the finest timescale, takes different values at each time step whereas processes M and P, which represent random fluctuations at an intermediate and a large timescale, may

have the same value for several time steps. This assumption was done for the sake of a simpler demonstration and it is not a structural assumption at all; without any change we could assume that M and P take different values at each time step, provided that their covariance structure remains Markovian with the same autocorrelation.

The above explanation may seem similar (from a practical point of view) to that by Klemes (1974), who attributed the Hurst phenomenon to non-stationary means. However, there is a fundamental difference here. As shown in the above analysis, we do not assume that means are nonstationary but rather, they are randomly varying at several scales. Nonstationarity of the mean would be the case if there existed a deterministic function expressing the mean as a function of time. Even though in some hydrologic texts (e.g., Kottegoda, 1980, p. 26), the falling or rising large-scale trends, traced in several hydrological time series, are classified as 'deterministic components' and are expressed as, say, linear functions of time, it is the author's opinion that these trends are not deterministic at all. For example, (as already discussed in section 3) the 25-year moving averages on the time series of Figure 1 indicate that there exist falling and rising large-scale trends but they follow an irregular random pattern rather than a regular deterministic one.

The conclusion of the above demonstration is that the nonstationarity notion is not necessary at all to explain the Hurst phenomenon. A stationary process can capture the Hurst effect and this agrees with Mandelbrot's notion. However, our explanation is contrary to the concept of long memory; the high autocorrelations appearing for high lags do not indicate long memory but they are a consequence of the large-scale random fluctuations as demonstrated with our simple example.

6. Simple algorithms to generate fractional Gaussian noise

As we have discussed in the introduction, several algorithms have been proposed to generate time series that respect the Hurst phenomenon. For some of these, the source code is widely available (e.g., the Splus programs by Beran, 1994, pp. 218-237). However, some of the known algorithms are not so simple both in understanding and implementation. Below we propose three much simpler algorithms that can be applied even in a spreadsheet environment.

These are based on the above-discussed properties of FGN and can be used to provide approximations of FGN good for practical hydrological purposes. In principle, all algorithms provided can be tuned to become as accurate as demanded. However, here we preferred to give emphasis to simplicity rather than accuracy. Theoretically, the algorithms can perform for any value of the Hurst exponent H in the interval (0, 1). However we have tested them on the subinterval (0.5, 1), which corresponds to the Hurst phenomenon (when $H < 0.5$ the autocorrelation function becomes negative for any lag, a case that is not met in hydrologic practice).

6.1 A multiple timescale fluctuation approach

In section 5 we saw that the weighted sum of three exponential functions of the time lag (equation (25)) can give an acceptable approximation of the autocorrelation function (equation (26)) of the FGN process at the basic timescale. This observation can lead to a (rather 'quick and dirty') algorithm to generate FGN. An extensive numerical investigation showed that the values of parameters ρ, φ, and ξ that appear in (26), which provide the best (in terms of mean square error) approximation of (18) are given by the following equations

$$\rho = 1.52\,(H-0.5)^{1.32}\,,\quad \varphi = 0.953 - 7.69\,(1-H)^{3.85},$$
$$\xi = \begin{cases} 0.932 + 0.087\,H & H \le 0.76 \\ 0.993 + 0.007\,H & H > 0.76 \end{cases} \tag{27}$$

The remaining parameters c_1 and c_2 can be then estimated such that the approximate autocorrelation function (26) match the exact function (18) for two lags, namely for lags 1 and 100. (Their values are obtained by solving two linear equations). Comparison plots of approximate autocorrelation functions based on equations (26) and (27) versus the exact autocorrelation functions of the FGN process for various values of the Hurst exponent H are shown in Figure 7.

In section 5 we also saw how to synthesise a process with the autocorrelation function (26) by assuming random changes of the mean on two timescales. However, there is a simpler way

to utilise (26) for generation of a time series. Specifically, (26) represents the sum of three independent AR(1) processes like that in (8), with lag one correlation coefficients ρ, φ, and ξ, and variances $(1 - c_1 - c_2)\,\gamma_0$, $c_1\,\gamma_0$, and $c_2\,\gamma_0$, respectively.

It must be mentioned that this algorithm is based essentially on the same principle with the fast fractional Gaussian noise (FFGN) algorithm (Mandelbrot, 1971); the differences are that it uses only 3 AR(1) components, much less than the FFGN, and the parameters of the algorithm are determined by the much simpler equation (27). Although the achieved approximation with the 3 AR(1) components is sufficient in practice for lags as high as 1000, it can be improved by increasing the number of the AR(1) components to 4, 5, etc. However, (27) will be not applicable then and the variances and lag one autocorrelations of the components must be estimated by minimising the mean squared departure of the composite autocorrelation function from that of the FGN process.

6.2 A disaggregation approach

The simple expressions of the statistics of the aggregated FGN process make possible a disaggregation approach for generating a time series of a FGN process. Specifically, let us assume that the desired length n of the synthetic series to be generated is 2^m where m is an integer (e.g., n = 2, 4, 8, 16, …; if n is not a power of 2 we can increase it to the next power of 2 and then discard the redundant generated items). We first generate the single value of $Z_1^{(n)}$ knowing that its variance is (from (17)) $n^{2H}\,\gamma_0$. Then we disaggregate $Z_1^{(n)}$ into two variables at the timescale n / 2, i.e. $Z_1^{(n/2)}$ and $Z_2^{(n/2)}$ and we proceed this way until the series $Z_1^{(1)} \equiv X_1$, …, $Z_n^{(1)} \equiv X_n$ is generated (see explanatory sketch on Figure 8).

The disaggregation algorithm that we propose reminds the midpoint displacement method (Saupe, 1988, p. 84) but is more accurate. It is based on a disaggregation technique introduced by Koutsoyiannis (2001). Since it is an induction technique it suffices to describe one step of the method application. Let us assume that we have completed the generation at the timescale $k \le n$ and we are generating the time series at the next timescale k / 2 (see Figure 8). We consider the generation step in which we disaggregate the higher-level amount $Z_i^{(k)}$ ($1 < i < n$ / k) into two lower-level amounts $Z_{2\,i-1}^{(k/2)}$ and $Z_{2\,i}^{(k/2)}$ such that

$$Z_{2i-1}^{(k/2)} + Z_{2i}^{(k/2)} = Z_i^{(k)} \tag{28}$$

Thus, it suffices to generate $Z_{2i-1}^{(k/2)}$ and then obtain $Z_{2i}^{(k/2)}$ from (28). At this generation step we have available the already generated values of previous lower-level time steps, i.e., $Z_1^{(k/2)}$, …, $Z_{2i-2}^{(k/2)}$ and of next higher-level time steps, i.e., $Z_{i+1}^{(k)}$, …, $Z_{n/k}^{(k)}$ (see explanatory sketch on Figure 8). Theoretically, it is necessary to preserve the correlations of $Z_{2i-1}^{(k/2)}$ with all previous lower-level variables and all next higher-level variables. However, we can get a very good approximation if we consider correlations with only one higher-level time step behind and one ahead. Under this simplification, $Z_{2i-1}^{(k/2)}$ can be generated from the linear relationship

$$Z_{2i-1}^{(k/2)} = a_2 Z_{2i-3}^{(k/2)} + a_1 Z_{2i-2}^{(k/2)} + b_0 Z_i^{(k)} + b_1 Z_{i+1}^{(k)} + V \tag{29}$$

where a_2, a_1, b_0 and b_1 are parameters to be estimated and V is innovation whose variance has to be estimated, too. All unknown parameters can be estimated in terms of correlations of the form $\mathrm{Corr}[Z_{2i-1}^{(k/2)}, Z_{2i-1+j}^{(k/2)}] = \rho_j$ where ρ_j is given by (18). Specifically, applying the methodology by Koutsoyiannis (2001) we find

$$\begin{bmatrix} a_2 \\ a_1 \\ b_0 \\ b_1 \end{bmatrix} = \begin{bmatrix} 1 & \rho_1 & \rho_2+\rho_3 & \rho_4+\rho_5 \\ \rho_1 & 1 & \rho_1+\rho_2 & \rho_3+\rho_4 \\ \rho_2+\rho_3 & \rho_1+\rho_2 & 2(1+\rho_1) & \rho_1+2\rho_2+\rho_3 \\ \rho_4+\rho_5 & \rho_3+\rho_4 & \rho_1+2\rho_2+\rho_3 & 2(1+\rho_1) \end{bmatrix}^{-1} \begin{bmatrix} \rho_2 \\ \rho_1 \\ 1+\rho_1 \\ \rho_2+\rho_3 \end{bmatrix} \tag{30}$$

and

$$\mathrm{Var}[V] = \gamma_0^{(k/2)} (1 - [\rho_2, \rho_1, 1+\rho_1, \rho_2+\rho_3]\,[a_2, a_1, b_0, b_1]^T) \tag{31}$$

where the superscript T denotes the transpose of a vector.

All parameters are independent of i and k and therefore they can be used in all steps. When $i = 1$ there are no previous time steps and thus the first two rows and columns of the above matrix and vectors are eliminated. Similarly, when $i = n / k$, there is no next time step and thus the last row and column of the above matrix and vectors are eliminated. The sequences of previous and past variables that are considered for generating each lower-level variable, and the related parameters, can be directly expanded, to increase the accuracy of the method.

However, as we will see in section 6.4, the above minimal configuration of the method gives satisfactory results.

6.3 A symmetric moving average approach

Koutsoyiannis (2000) introduced the so call symmetric moving average (SMA) generating scheme that can be used to generate any kind of stochastic process with any autocorrelation structure or power spectrum. Like the conventional (backward) moving average (MA) process, the SMA scheme transforms a white noise sequence V_i into a process with autocorrelation by taking the weighted average of a number of V_i. In the SMA process the weights a_j are symmetric about a centre (a_0) that corresponds to the variable V_i, i.e.,

$$X_i = \sum_{j=-q}^{q} a_{|j|}\, V_{i+j} = a_q\, V_{i-q} + \ldots + a_1\, V_{i-1} + a_0\, V_i + a_1\, V_{i+1} + \ldots + a_q\, V_{i+q} \qquad (32)$$

where q theoretically is infinity but in practice can be restricted to a finite number, as the sequence of weights a_j tends to zero for increasing j. The autocovariance implied by (32) is

$$\gamma_j = \sum_{l=-q}^{q-j} a_{|l|}\, a_{|j+l|}, \qquad j = 0, 1, 2, \ldots \qquad (33)$$

Koutsoyiannis (2000) also showed that the discrete Fourier transform $s_a(\omega)$ of the a_j sequence is related to the power spectrum of the process $s_\gamma(\omega)$ by

$$s_a(\omega) = \sqrt{2\, s_\gamma(\omega)} \qquad (34)$$

This enables the direct calculation of $s_a(\omega)$, which in the case of FGN, given (22), will be

$$s_a(\omega) \approx 2\sqrt{(2 - 2\,H)\,\gamma_0}\,(2\,\omega)^{0.5-H} \qquad (35)$$

Comparing (22) and (35) we observe that $s_a(\omega)$ is approximately equal to the power spectrum of another FGN process with Hurst exponent $H' = (H + 0.5)/2$ and variance $[\sqrt{2 - 2\,H}\,/\,(1.5 - H)]\,\sqrt{\gamma_0}$. Consequently, we can use (18) to approximate the inverse Fourier transform of $s_a(\omega)$, i.e., the sequence of a_j itself:

$$a_j \approx \frac{\sqrt{(2-2H)\,\gamma_0}}{3-2H}\,[(j+1)^{H+0.5} + (j-1)^{H+0.5} - 2j^{H+0.5}], \quad j > 0 \tag{36}$$

In conclusion, the generation scheme (32) with coefficients a_j determined from (36) can lead to a very easy algorithm for generating FGN. This method can also preserve the process skewness ξ_X by appropriately choosing the skewness of the white noise ξ_V. The relevant equations for the statistics of V_i, which are direct consequences of (32), are

$$\left(a_0 + 2\sum_{j=1}^{s} a_j\right) E[V_i] = \mu, \quad \mathrm{Var}[V_i] = 1, \quad \left(a_0^3 + 2\sum_{j=1}^{q} a_j^3\right) \xi_V = \xi_X \gamma_0^{3/2} \tag{37}$$

Given that the weights a_j are $q + 1$ in total, the model can preserve the first $q + 1$ terms of the autocovariance γ_j of the process X_i. Thus, the number q must be chosen at least equal to the desired number of autocorrelation coefficients m that are to be preserved. In addition, the ignored terms a_j beyond a_q must not exceed an acceptable tolerance $\beta\sqrt{\gamma_0}$. These two conditions in combination with (19) and (36) result in

$$q \geq \max\left[m, \left(\frac{2\beta}{H^2 - 0.25}\right)^{1/(H-1.5)}\right] \tag{38}$$

The number q can be very large (on the order of thousands to hundred of thousands) if H is large (e.g. > 0.9) and β is small (e.g. < 0.001). Approximate autocorrelation functions for lags up to m = 10 000 based on equations (32) and (36) versus the exact autocorrelation functions of the FGN process for various values of the Hurst exponent H and the number of weights q are shown in Figure 9.

The accuracy of the method depends on the number q. However, even when $q \to \infty$ the method does not become exact because of the approximate character of (36). Although more accurate estimates the a_j series can be obtained numerically by a method by Koutsoyiannis (2000), the estimates given by (36) are sufficiently accurate for practice. This is verified in Figure 9 where theoretical and approximate autocorrelation functions are almost indistinguishable.

6.4 Demonstration of the methods

The three proposed methods for generating FGN are demonstrated by synthesising records with length, mean, variance and Hurst exponent equal to those of the historical standardised tree rings series at Mammoth Creek, Utah. The generated synthetic records using all three methods are plotted in Figure 10. In comparison with the original series of Figure 1 (middle) we observe that all three series exhibit a similar general shape with the same fluctuation amplitudes at all plotted timescales (1, 5 and 25 years). Figure 11 depicts the standard deviation of the aggregated processes $Z_i^{(k)}$ versus timescale k for the three synthetic time series generated. For comparison we have also plotted the theoretical curves of the white noise and FGN models. We observe that all three empirical curves are straight lines on the logarithmic plots with slope 0.75, i.e., equal to the assumed Hurst exponent. Figure 12 depicts the autocorrelation functions of the three synthetic time series on the basic (annual) scale for lags up to 50. For comparison we have also plotted the theoretical curves of the AR(1) and FGN models. We observe that the empirical autocorrelation functions of all three synthetic samples are close to the theoretical ones of the FGN process with $H = 0.75$. Some departures are due to sampling errors as the record length of 1990 values is too small to accurately estimate autocorrelations for lags as high as 50. To verify this, we also generated three additional synthetic records with lengths 64 000 values and plotted their autocorrelation functions on Figure 12, too. We observe that the empirical autocorrelation functions of the latter series are almost indistinguishable from the theoretical ones of the FGN process. In conclusion, this demonstration shows that all three methods are good for practical purposes.

7. Conclusions and discussion

A first conclusion of this paper is that the Hurst phenomenon can be formulated and studied in an easy manner in terms of the variance and autocorrelation of a stochastic process on multiple timescales, thus avoiding the use of the complicated concept of rescaled range (see Appendix A1). In addition, the Hurst phenomenon can have a simple and easily understandable explanation based on the random fluctuation of a hydrologic process upon

different timescales. A second conclusion is that the generation of the fractional Gaussian noise, the process that reproduces the Hurst phenomenon, can be performed by either of three simple proposed methods that are based on (a) a multiple timescale fluctuation approach, (b) a disaggregation approach, and (c) a symmetric moving average approach.

Among these three methods, (a) and (b) are very fast as the required computer time on a common Pentium PC is of the order of tens of milliseconds (for the applications presented in section 6.4); this becomes of the order of seconds for method (c). Methods (b) and (c) can be directly extended to generate multivariate series as well (for a general framework of such adaptations for methods (b) and (c), see Koutsoyiannis, 2001 and 2000, respectively). Methods (a) and (c) can generate series with skewed distributions. Method (c) is the most accurate but the other methods are sufficiently accurate and can be directly adapted to further improve accuracy, as discussed in section 6. In general, all three methods are good for practical hydrological purposes. Method (a) may be preferable for single variate problems with symmetric or asymmetric distributions. Method (b) is best for single-variate or multivariate problems with normal distribution. Finally, method (c) is good for any kind of problems, single-variate or multivariate with symmetric or asymmetric distributions but it is slower than the other ones.

Obviously, the FGN process with its singe parameter H is a simplified model of reality. Therefore, it may be not appropriate for all hydroclimatic series, even though it is much more consistent with reality in comparison with the AR and ARMA process. A generalised and comprehensive family of processes, which can include a larger number of parameters and incorporates both the FGN and the ARMA processes, has been studied by Koutsoyiannis (2000).

Appendix A1: Additional material related to the range concept

In hydrologic texts, the Hurst phenomenon and related topics are analysed in terms of several storage-related families of random variables (e.g., Yevjevich, 1972; Kottegoda, 1980, p. 184; Salas, 1993, p. 19.14) like the partial sum

$$Y_n := X_1 + X_2 + \ldots + X_n \tag{39}$$

of the stochastic process X_i (i = 1, 2, …), for any integer n; the range

$$R_n := \max(Y_i - i\,\mu; 1 \le i \le n) - \min(Y_i - i\,\mu; 1 \le i \le n) \tag{40}$$

the adjusted range

$$R_n^* := \max(Y_i - i\,Y_n / n; 1 \le i \le n) - \min(Y_i - i\,Y_n / n; 1 \le i \le n) \tag{41}$$

where the true mean μ has been replaced by the sample mean Y_n / n; and the rescaled range

$$R_n^{**} = R_n^* / S_n \tag{42}$$

where S_n is the sample standard deviation of $X_1, X_2, \ldots, X_n$. We emphasise that R_n, R_n^* and R_n^{**} are random variables whose distribution depends on the distribution of X_i, the number n and the covariance structure of the process $X_1, X_2, \ldots, X_n$. The study of the distribution of R_n, R_n^*, and particularly R_n^{**}, is a very complicated task. Even their means are difficult to estimate accurately (Yevjevich, 1972, pp. 148-173). For instance, in the simple case where $X_1, X_2, \ldots, X_n$ are independent normal variables with known μ and σ, the mean range is (Yevjevich, 1972, p. 151)

$$E[R_n] = \sigma \sqrt{\frac{2}{\pi}} \sum_{i=1}^{n} \frac{1}{\sqrt{i}} \tag{43}$$

and in the yet simple case where X_i is an AR(1) Gaussian process with known μ and σ, the mean range is (Yevjevich, 1972, p. 158)

$$E[R_n] = \sigma \sqrt{\frac{2}{\pi (1-\rho^2)}} \sum_{i=1}^{n} \sqrt{\frac{1+\rho}{i (1-\rho)} - \frac{2\rho (1-\rho^i)}{i^2 (1-\rho)^2}} \tag{44}$$

(Interestingly, (44) is displayed on the cover of the book by Yevjevich (1972)).

For R_n^* and R_n^{**}, only approximate relations have been known. For example the mean adjusted range in the simple case where $X_1, X_2, \ldots, X_n$ are independent normal variables with known μ and σ, Yevjevich (1972, p. 152) presents the following equation, obtained by Monte Carlo simulation using 100 000 independent standard normal numbers:

$$E[R_n^*] \approx \sigma \left(\sqrt{\frac{\pi n}{2}} - \sqrt{\frac{\pi}{2}} \right) \tag{45}$$

Generally, it is known that for all ARMA type processes, the rescaled range is asymptotically

$$E[R_n^{**}] \approx c \sqrt{n} \tag{46}$$

and for the FGN process

$$E[R_n^{**}] \approx c\, n^H \tag{47}$$

where c is a constant (e.g., Bras and Rodriguez-Iturbe, 1985, p. 221).

Equation (47) has been traditionally used to estimate the Hurst coefficient. However, the uncertainty implied by (47) is very high. It suffices to say that H can result greater than one (for example, see Figures 7 and 8 in Vogel et al., 1998), which is not allowed theoretically.

From a conceptual point of view, the range concept corresponds to the mass curve analysis of a reservoir (plot of cumulated inflows and outflows), a graphical method first developed by Ripple in 1883 and widely used in reservoir design since then. In this regard, R_n represents the required storage of a reservoir operating without any spill or other loss and providing a constant outflow equal to the mean flow. Obviously, this is an oversimplification of a real reservoir. Therefore, this method needs to be abandoned today and the range concept needs to be replaced by probability-based design methods.

Because of the complications in definition and conceptualisation of the different range concepts, the complex relationships of their statistical properties, and the estimation problems,

we have avoided using these concepts in the paper. As shown in the paper, the concept of variance (or standard deviation) on multiple timescales is a much simpler and more accurate approach, which does not require the range concept at all. However, for the sake of compatibility with previous studies we have included in this appendix a set of figures related to the range concept.

Thus, in Figure 13 we have plotted the mean rescaled range R_n^{**} as a function of length n for the two example historical time series of section 3. We observe that (47) is validated with $H = 0.88$ for the Nile time series and $H = 0.74$ for the Utah time series. These values are close to the already estimated values (section 3 and Figure 2), $H = 0.85$ and $H = 0.75$, respectively.

In addition, in Figure 14 we have plotted the mean rescaled range R_n^{**} as a function of length n for the synthetic time series generated in section 6.4. We observe that the slopes of the empirical curves of R_n^{**} versus n on the logarithmic plot are close to the theoretical expectation $H = 0.75$.

Appendix A2: Derivation of (18)

We observe that

$$Z_1^{(kj+k)} = Z_1^{(kj)} + Z_{j+1}^{(k)} \tag{48}$$

and consequently

$$\mathrm{Var}[Z_1^{(kj+k)}] = \mathrm{Var}[Z_1^{(kj)}] + \mathrm{Var}[Z_{j+1}^{(k)}] + 2\,\mathrm{Cov}[Z_1^{(kj)}, Z_{j+1}^{(k)}] \tag{49}$$

From (17) we get

$$\mathrm{Var}[Z_1^{(kj+k)}] = \left(\frac{kj+k}{k}\right)^H \mathrm{Var}[Z_1^{(k)}], \quad \mathrm{Var}[Z_1^{(kj)}] = \left(\frac{kj}{k}\right)^H \mathrm{Var}[Z_1^{(k)}] \tag{50}$$

and we conclude that

$$\mathrm{Cov}[Z_1^{(kj)}, Z_{j+1}^{(k)}] = (\mathrm{Var}[Z_1^{(k)}] / 2)\,[(j+1)^{2H} - j^{2H} - 1] \tag{51}$$

Besides,

$$Z_1^{(kj)} = \sum_{i=1}^{j} Z_i^{(k)} \tag{52}$$

so that

$$\mathrm{Cov}[Z_1^{(kj)}, Z_{j+1}^{(k)}] = \mathrm{Var}[Z_1^{(k)}] \sum_{i=1}^{j} \rho_i^{(k)} \tag{53}$$

and thus

$$\sum_{i=1}^{j} \rho_i^{(k)} = (1/2)\,[(j+1)^{2H} - j^{2H} - 1] \tag{54}$$

Likewise,

$$\sum_{i=1}^{j-1} \rho_i^{(k)} = (1/2)\,[j^{2H} - (j-1)^{2H} - 1] \tag{55}$$

Subtracting (55) from (54) we get (18).

Acknowledgments. The research leading to this paper was performed within the framework of the project *Modernization of the supervision and management of the water resource system of Athens*, funded by the Water Supply and Sewage Corporation of Athens. The author wishes to thank the directors of the Corporation and the members of the project committee for the support of the research. Thanks are also due to I. Nalbantis for his comments.

References

Abry, P., P. Gonçalvés and P. Flandrin (1995). Wavelets, spectrum analysis and 1/*f* processes, in *Wavelets and Statistics*, edited by A. Antoniadis and G. Oppenheim, Springer-Verlag, New York.

Bak, P. (1996). *How Nature Works, The Science of Self-Organized Criticality*, Copernicus, Springer-Verlag, New York.

Beran, J. (1994). *Statistics for Long-Memory Processes*, Volume 61 of *Monographs on Statistics and Applied Probability*, Chapman and Hall, New York.

Bhattacharya, R, N., V. K. Gupta and E. Waymire (1983). The Hurst effect under trends, *J. Appl. Prob.*, 20, 649-662.

Bloomfield, P. (1976). *Fourier Analysis of Time Series*, Wiley, New York.

Bloomfield, P. (1992). Trends in global temperature, *Climate Change*, 21, 1-16.

Box, G. E. P., G. M. Jenkins and G. C. Reinsel (1994). *Time Series Analysis, Forecasting and Control*, Prentice Hall, Upper Saddle River, New Jersey.

Bras, R.L. and I. Rodriguez-Iturbe (1985). *Random Functions in Hydrology*, Addison-Wesley.

Debnath, L. (1995). *Integral Transforms and Their Applications*, CRC Press, New York.

Ditlevsen, O. D. (1971). Extremes and first passage times, Doctoral dissertation presented to the Technical University of Denmark, Lyngby, Denmark.

Eltahir, E. A. B. (1996). El Niño and the natural variability in the flow of the Nile River, *Water Resources Research*, 32(1) 131-137.

Evans, T. E. (1996). The effects of changes in the world hydrological cycle on availability of water resources, Chapter 2 in *Global Climate Change and Agricultural Production: Direct and Indirect Effects of Changing Hydrological, Pedological and Plant Physiological Processes*, edited by F. Bazzaz and W. Sombroek, Food and Agriculture Organization of the United Nations and John Wiley, Chichester.

Graybill, D. A., (1990). IGBP PAGES/World Data Center for Paleoclimatology, NOAA/NGDC Paleoclimatology Program, Boulder, Colorado, USA.

Grygier, J. C. and J. R. Stedinger, (1990). SPIGOT, A synthetic streamflow generation software package, Technical description, School of Civil and Environmental Engineering, Cornell University, Ithaca, NY., Version 2.5.

Haan C.T. (1977). *Statistical Methods in Hydrology*, Iowa State University Press, Ames, 378 pp.

Haslett, J., and A. E. Raftery (1989). Space-time modelling with long-memory dependence: Assessing Ireland's wind power resource, *Appl. Statist.*, 38(1), 1-50.

Hosking, J. R. M. (1981). Fractional differencing, *Biometrica*, 68, 165-176.

Hosking, J. R. M. (1984). Modeling persistence in hydrological time series using fractional differencing, *Water Resources Research*, 20(12) 1898-1908.

Hurst, H. E. (1951). Long term storage capacities of reservoirs, *Trans. ASCE*, 116, 776-808.

Klemes, V. (1974). The Hurst phenomenon: A puzzle?, *Water Resour. Res.*, 10(4) 675-688.

Kottegoda, N. T. (1980). *Stochastic Water Resources Technology*, Macmillan Press, London.

Koutsoyiannis, D., (2000). A generalized mathematical framework for stochastic simulation and forecast of hydrologic time series, *Water Resources Research*, 36(6), 1519-1534.

Koutsoyiannis, D., Coupling stochastic models of different time scales, *Water Resources Research*, 37(2), 379-392, 2001.

Lane, W. L. and D. K. Frevert (1990). Applied Stochastic Techniques, User's Manual, Bureau of Reclamation, Engineering and Research Center, Denver, Co., Personal Computer Version.

Mandelbrot, B. B. (1965). Une class de processus stochastiques homothetiques a soi: Application a la loi climatologique de H. E. Hurst, *Compte Rendus Academie Science*, 260, 3284-3277.

Mandelbrot, B. B. (1971). A fast fractional Gaussian noise generator, *Water Resour. Res.*, 7(3), 543-553.

Mandelbrot, B. B. (1977). *The Fractal Geometry of Nature*, Freeman, New York.

Mandelbrot, B. B., and J. R. Wallis (1969a). Computer experiments with fractional Gaussian noises, Part 1, Averages and variances, *Water Resour. Res.*, 5(1), 228-241.

Mandelbrot, B. B., and J. R. Wallis (1969b). Computer experiments with fractional Gaussian noises, Part 2, Rescaled ranges and spectra, *Water Resour. Res.*, 5(1), 242-259.

Mandelbrot, B. B., and J. R. Wallis (1969c). Computer experiments with fractional Gaussian noises, Part 3, Mathematical appendix, *Water Resour. Res.*, 5(1), 260-267.

Mejia, J. M., I. Rodriguez-Iturbe and D. R. Dawdy (1972). Streamflow simulation, 2, The broken line process as a potential model for hydrologic simulation, *Water Resour. Res.*, 8(4), 931-941.

Mesa, O. J., and G. Poveda (1993). The Hurst effect: The scale of fluctuation approach, *Water Resour. Res.*, 29(12), 3995-4002.

Montanari, A., R. Rosso and M. S. Taqqu (1997). Fractionally differenced ARIMA models applied to hydrologic time series, *Water Resour. Res.*, 33(5), 1035-1044.

National Research Council, (1991). Committee on Opportunities in the Hydrologic Sciences, *Opportunities in the Hydrologic Sciences*, National Academy Press, Washington, DC.

Papoulis, A. (1991). *Probability, Random Variables, and Stochastic Processes*, 3rd ed., McGraw-Hill, New York.

Radziejewski, M., and Z. W. Kundzewicz (1997). Fractal analysis of flow of the river Warta, *J. of Hydrol.*, 200, 280-294.

Salas, J. D. (1993). Analysis and modeling of hydrologic time series, *Handbook of Hydrology*, edited by D. Maidment, Chapter 19, pp. 19.1-19.72, McGraw-Hill, New York.

Salas, J. D., and D. C. Boes (1980). Shifting level modelling of hydrologic time series, *Advances in Water Resources*, 3, 59-63.

Salas, J. D., J. W. Delleur, V. Yevjevich, and W. L. Lane (1980). *Applied Modeling of Hydrologic Time Series*, Water Resources Publications, Littleton, Colorado.

Saupe, D. (1988). Algorithms for random fractals, Chapter 2 in *The Science of Fractal Images*, edited by H.-O. Peitgen and D. Saupe, Springer-Verlag.

Stephenson, D. B., V. Pavan and R. Bojariu (2000). Is the North Atlantic Oscillation a random walk?, *Int. J. Climatol.*, 20, 1-18.

Toussoun, O. (1925). Mémoire sur l'histoire du Nil, in *Mémoires a l'Institut d'Egypte*, vol. 18, pp. 366-404.

Vanmarke, E. (1983). *Random Fields*, The MIT Press, Cambridge, Mass.

Vogel, R. M., Y. Tsai and J. F. Limbrunner (1998). The regional persistence and variability of annual streamflow in the United States, *Water Resour. Res.*, 34(12), 3445-3459.

Yevjevich, V. (1972). *Stochastic Processes in Hydrology*, Water Resources Publications, Fort Collins, Colorado.

List of Figures

Figure 1 Plots of the two example time series: (up) annual minimum water level of Nile; (middle) standardised tree rings at Mammoth Creek, Utah. For comparison we have also plotted (down) a series of white noise with statistics same with those of standardised tree rings.

Figure 2 Standard deviation of the aggregated processes $Z_i^{(k)}$ versus timescale k (logarithmic plots) for the two example data sets: (up) annual minimum water level of Nile; (down) standardised tree rings at Mammoth Creek, Utah. For comparison we have also plotted theoretical curves for the white noise and AR(1) models.

Figure 3 Lag one and lag two autocorrelation coefficients of the aggregated processes $Z_i^{(k)}$ versus timescale k for the two example data sets: (up) annual minimum water level of Nile; (down) standardised tree rings at Mammoth Creek, Utah. For comparison we have also plotted the theoretical curves of the AR(1) model.

Figure 4 Autocorrelation functions of the two example time series at the basic (annual) scale: (up) annual minimum water level of Nile; (down) standardised tree rings at Mammoth Creek, Utah. For comparison we have also plotted the theoretical curves of the AR(1) model.

Figure 5 Illustrative sketch for multiple timescale random fluctuations of a process that can explain the Hurst phenomenon: (a) a time series from a Markovian process with constant mean; (b) the same time series superimposed to a randomly fluctuating mean at a medium timescale; (c) the same time series further superimposed to a randomly fluctuating mean at a large timescale.

Figure 6 Plots of the example autocorrelation functions of (a) the Markovian process U with constant mean; (b) the process U superimposed to a randomly fluctuating mean at a medium timescale (process V); (c) the process V further superimposed to a randomly fluctuating mean at a large timescale (process W). The superimposition of fluctuating means increases the lag

one autocorrelation (from $\rho_1 = 0.20$ for U to $\rho_1 = 0.30$ and 0.33 for V and W respectively) and also shifts the autocorrelation function from the AR(1) shape (also plotted in all three panels) towards the FGN shape (also shown in all three panels).

Figure 7 Approximate autocorrelation functions based on equations (26) and (27) versus the exact autocorrelation functions of the FGN process for various values of the Hurst exponent H.

Figure 8 Explanation sketch for the disaggregation approach for generation of a FGN time series. Grey boxes indicate random variables whose values have been already generated prior to the current step and arrows indicate the links to those of the generated variables that are considered in the current generation step.

Figure 9 Approximate autocorrelation functions based on equations (32) and (36) versus the exact autocorrelation functions of the FGN process for various values of the Hurst exponent H and the number of weights q.

Figure 10 Plots of the three synthetic time series generated using the statistics of standardised tree rings at Mammoth Creek, Utah, and implementing: (up) the multiple timescale fluctuation approach; (middle) the disaggregation approach; (down) the symmetric moving average approach.

Figure 11 Standard deviation of the aggregated processes $Z_i^{(k)}$ versus timescale k (logarithmic plots) for the three synthetic time series generated using: (up) the multiple timescale fluctuation approach; (middle) the disaggregation approach; (down) the symmetric moving average approach. For comparison we have also plotted the theoretical curves of the white noise and FGN models.

Figure 12 Autocorrelation functions of the three synthetic time series at the basic (annual) scale generated using: (up) the multiple timescale fluctuation approach; (middle) the disaggregation approach; (down) the symmetric moving average approach. For comparison we have also plotted the theoretical curves of the AR(1) and FGN models and empirical

functions of three additional series with large length (64 000) generated using the same three methods.

Figure 13 Mean rescaled range $E[R_k^{**}]$ versus time length k (logarithmic plots) for the two example historical data sets: (up) annual minimum water level of Nile; (down) standardised tree rings at Mammoth Creek, Utah. For comparison we have also plotted approximate theoretical curves for the white noise and FGN models.

Figure 14 Mean rescaled range $E[R_k^{**}]$ versus time length k (logarithmic plots) for the three synthetic time series generated using: (up) the multiple timescale fluctuation approach; (middle) the disaggregation approach; (down) the symmetric moving average approach. For comparison we have also plotted approximate theoretical curves for the white noise and FGN models.

Figures

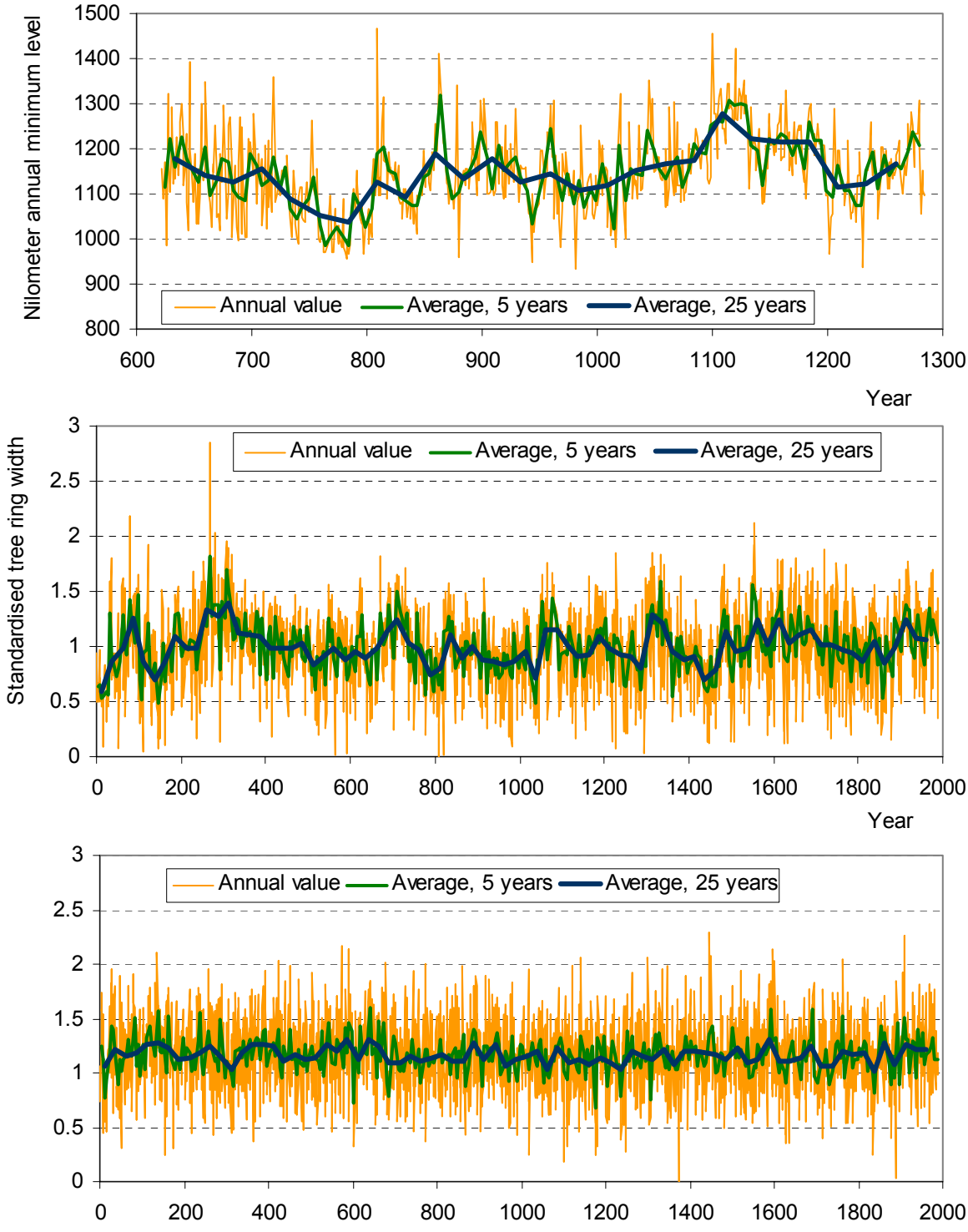

Figure 1 Plots of the two example time series: (up) annual minimum water level of Nile; (middle) standardised tree rings at Mammoth Creek, Utah. For comparison we have also plotted (down) a series of white noise with statistics same with those of standardised tree rings.

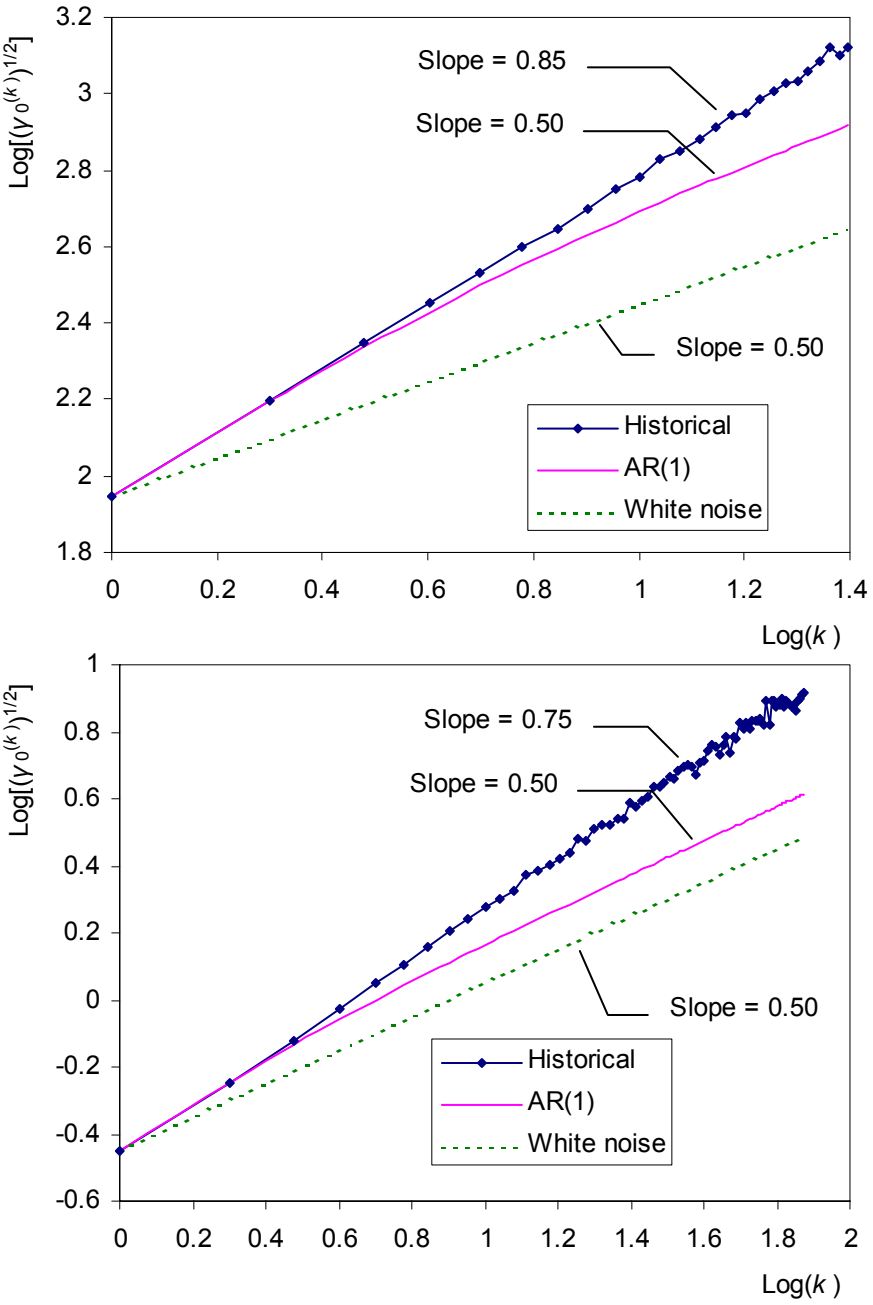

Figure 2 Standard deviation of the aggregated processes $Z_i^{(k)}$ versus timescale k (logarithmic plots) for the two example data sets: (up) annual minimum water level of Nile; (down) standardised tree rings at Mammoth Creek, Utah. For comparison we have also plotted theoretical curves for the white noise and AR(1) models.

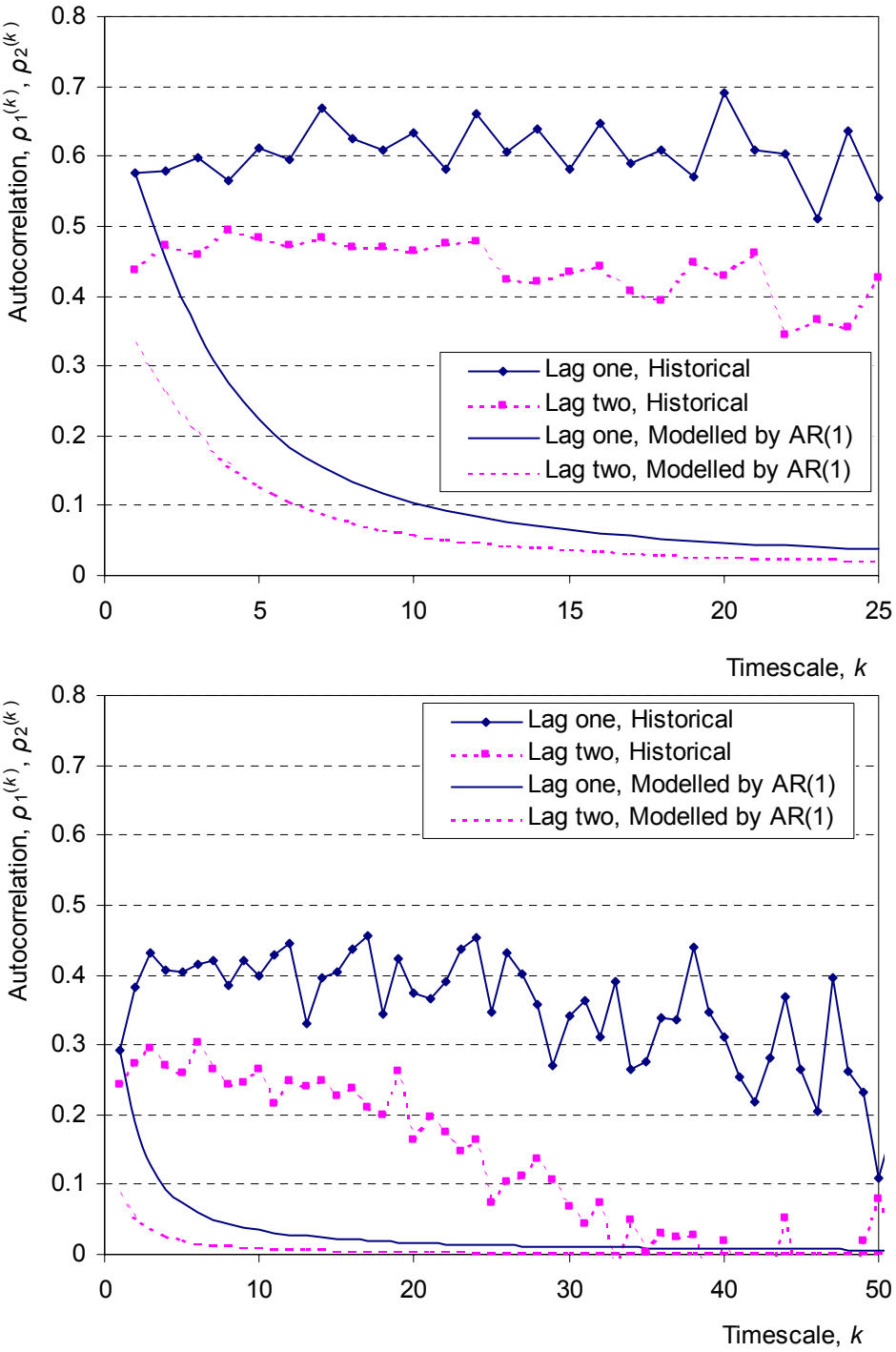

Figure 3 Lag one and lag two autocorrelation coefficients of the aggregated processes $Z_i^{(k)}$ versus timescale k for the two example data sets: (up) annual minimum water level of Nile; (down) standardised tree rings at Mammoth Creek, Utah. For comparison we have also plotted the theoretical curves of the AR(1) model.

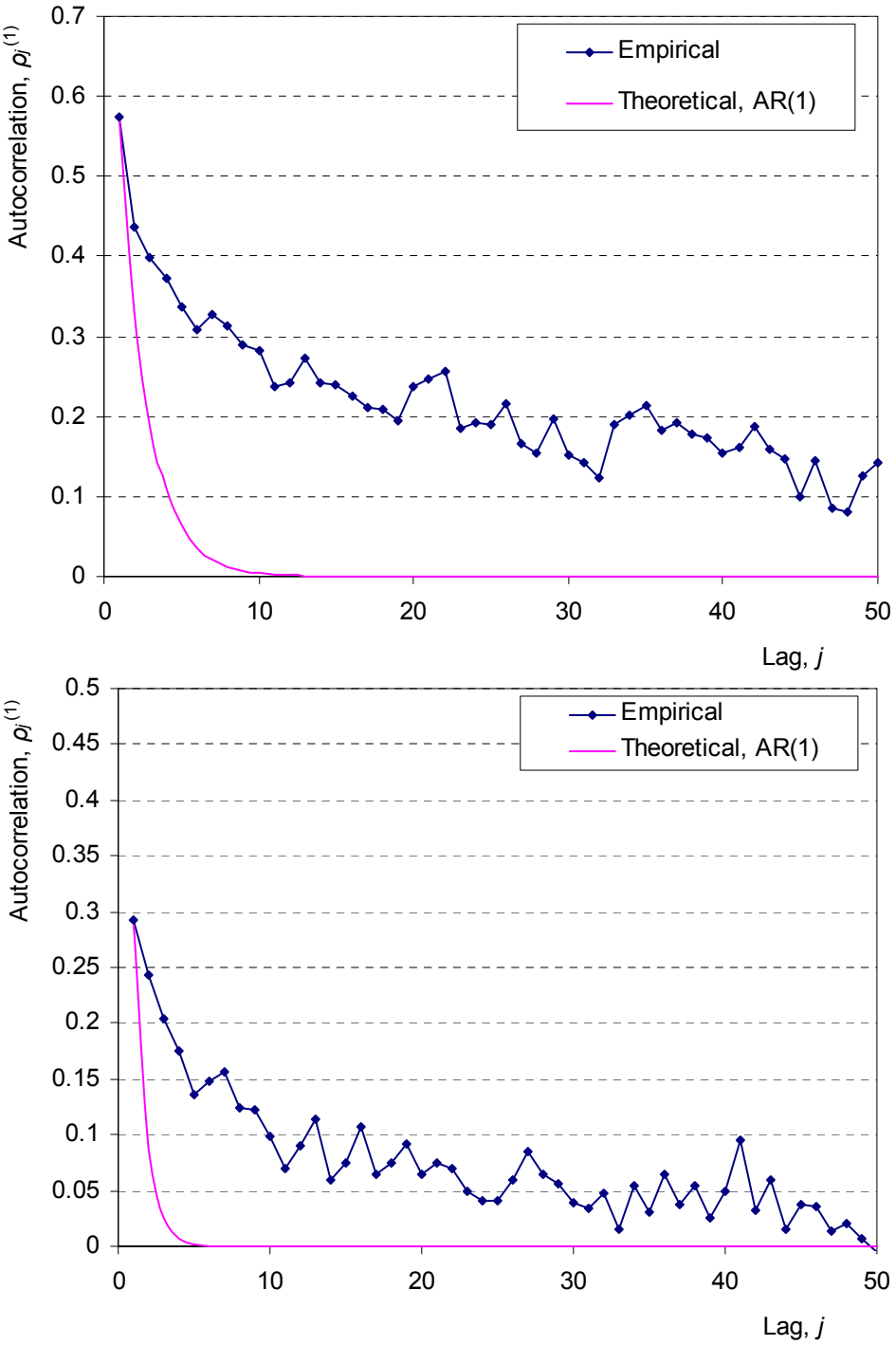

Figure 4 Autocorrelation functions of the two example time series at the basic (annual) scale: (up) annual minimum water level of Nile; (down) standardised tree rings at Mammoth Creek, Utah. For comparison we have also plotted the theoretical curves of the AR(1) model.

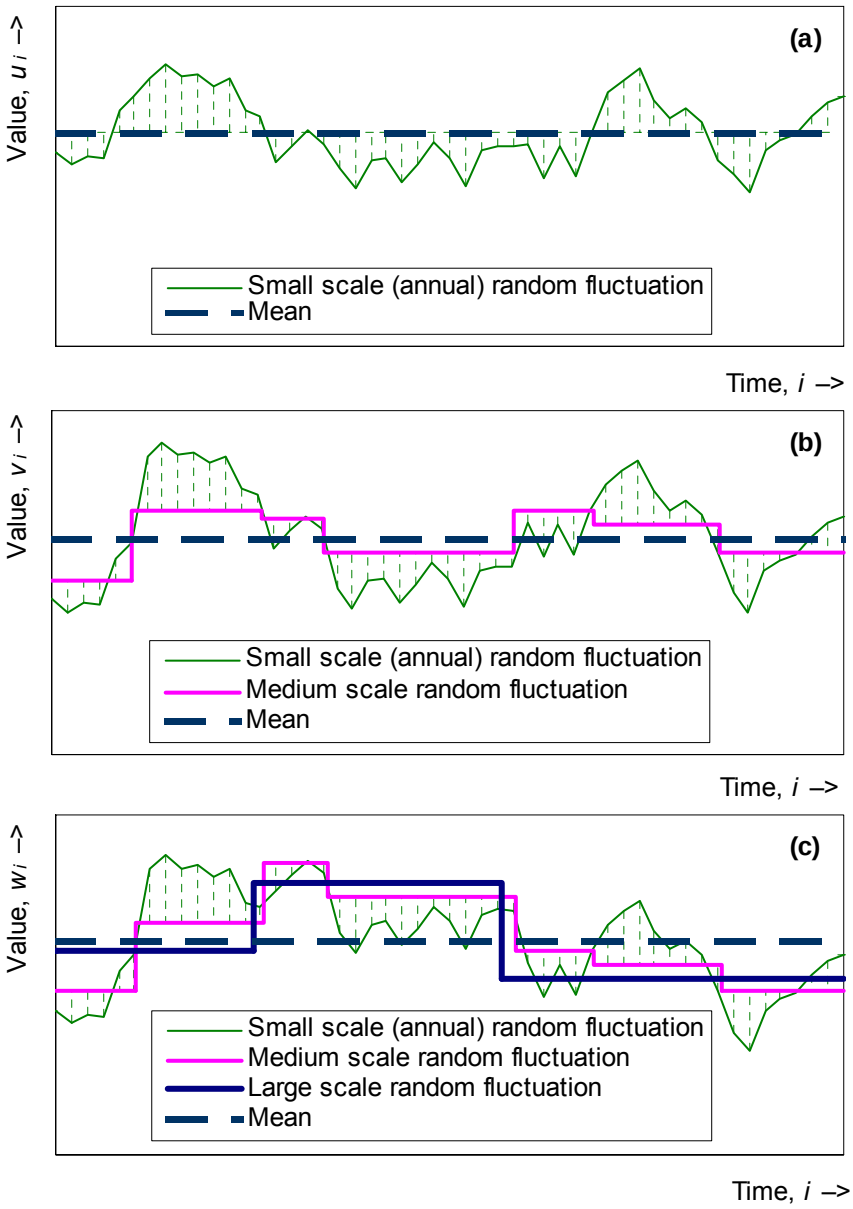

Figure 5 Illustrative sketch for multiple timescale random fluctuations of a process that can explain the Hurst phenomenon: (a) a time series from a Markovian process with constant mean; (b) the same time series superimposed to a randomly fluctuating mean at a medium timescale; (c) the same time series further superimposed to a randomly fluctuating mean at a large timescale.

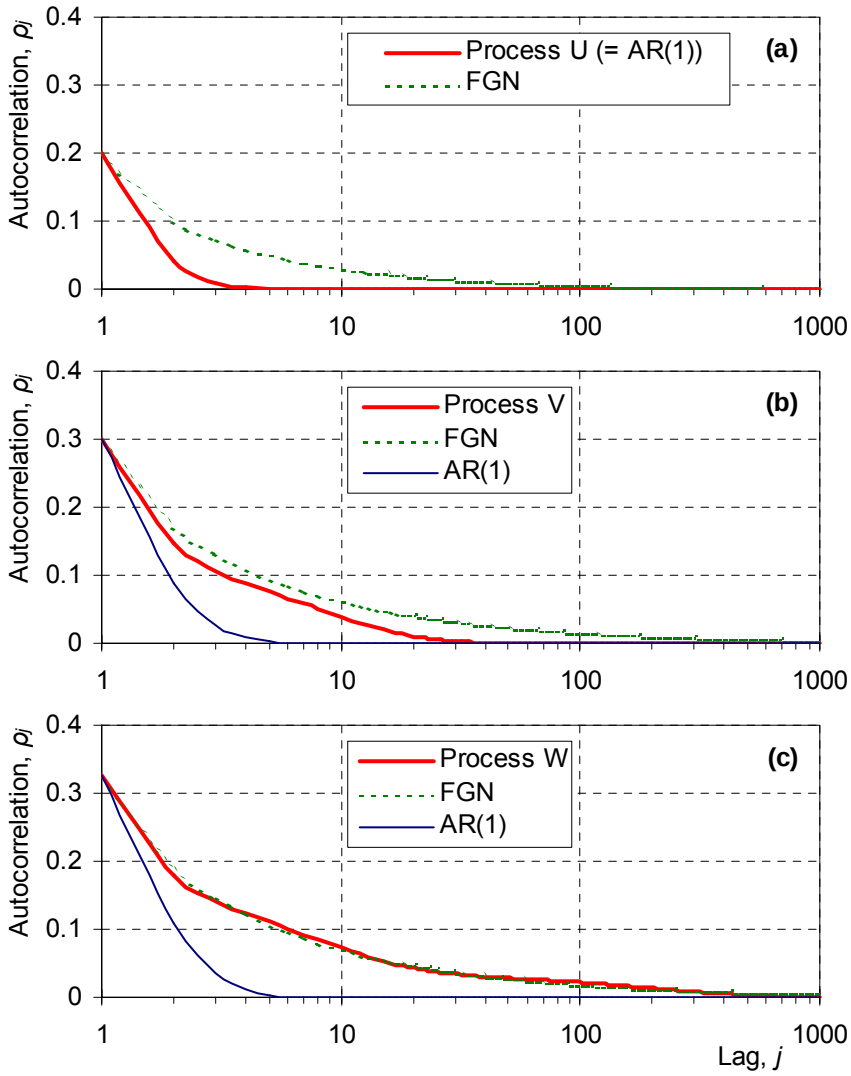

Figure 6 Plots of the example autocorrelation functions of (a) the Markovian process *U* with constant mean; (b) the process *U* superimposed to a randomly fluctuating mean at a medium timescale (process *V*); (c) the process *V* further superimposed to a randomly fluctuating mean at a large timescale (process *W*). The superimposition of fluctuating means increases the lag one autocorrelation (from $\rho_1 = 0.20$ for *U* to $\rho_1 = 0.30$ and 0.33 for *V* and *W* respectively) and also shifts the autocorrelation function from the AR(1) shape (also plotted in all three panels) towards the FGN shape (also shown in all three panels).

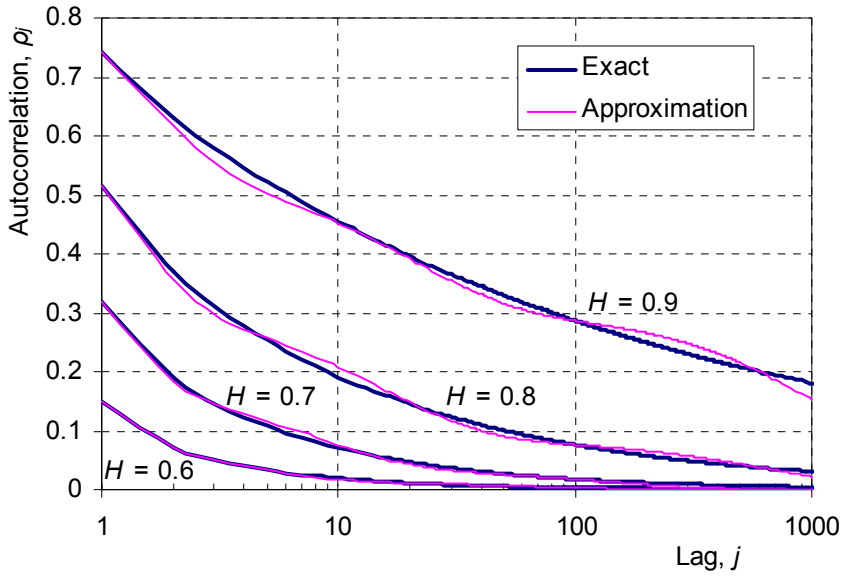

Figure 7 Approximate autocorrelation functions based on equations (26) and (27) versus the exact autocorrelation functions of the FGN process for various values of the Hurst exponent H.

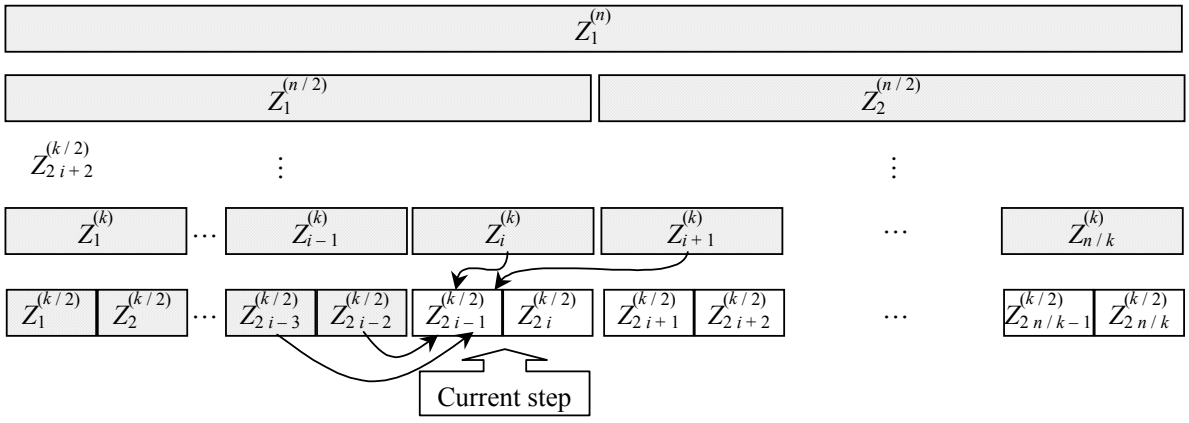

Figure 8 Explanation sketch for the disaggregation approach for generation of a FGN time series. Grey boxes indicate random variables whose values have been already generated prior to the current step and arrows indicate the links to those of the generated variables that are considered in the current generation step.

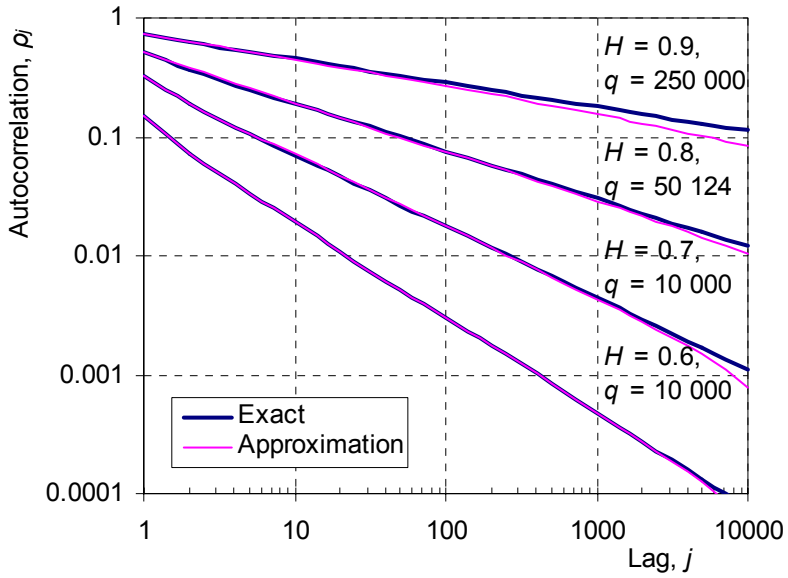

Figure 9 Approximate autocorrelation functions based on equations (32) and (36) versus the exact autocorrelation functions of the FGN process for various values of the Hurst exponent H and the number of weights q.

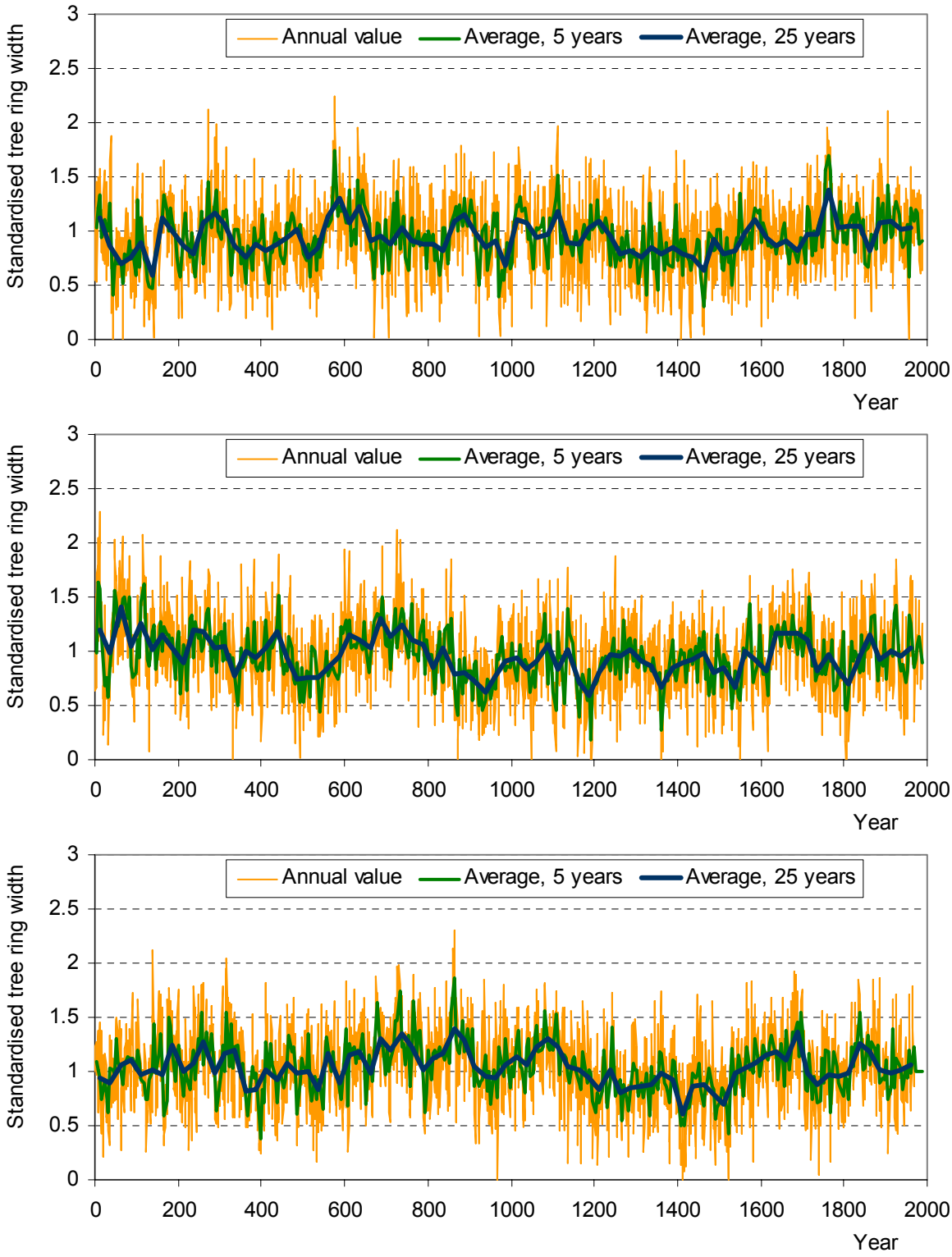

Figure 10 Plots of the three synthetic time series generated using the statistics of standardised tree rings at Mammoth Creek, Utah, and implementing: (up) the multiple timescale fluctuation approach; (middle) the disaggregation approach; (down) the symmetric moving average approach.

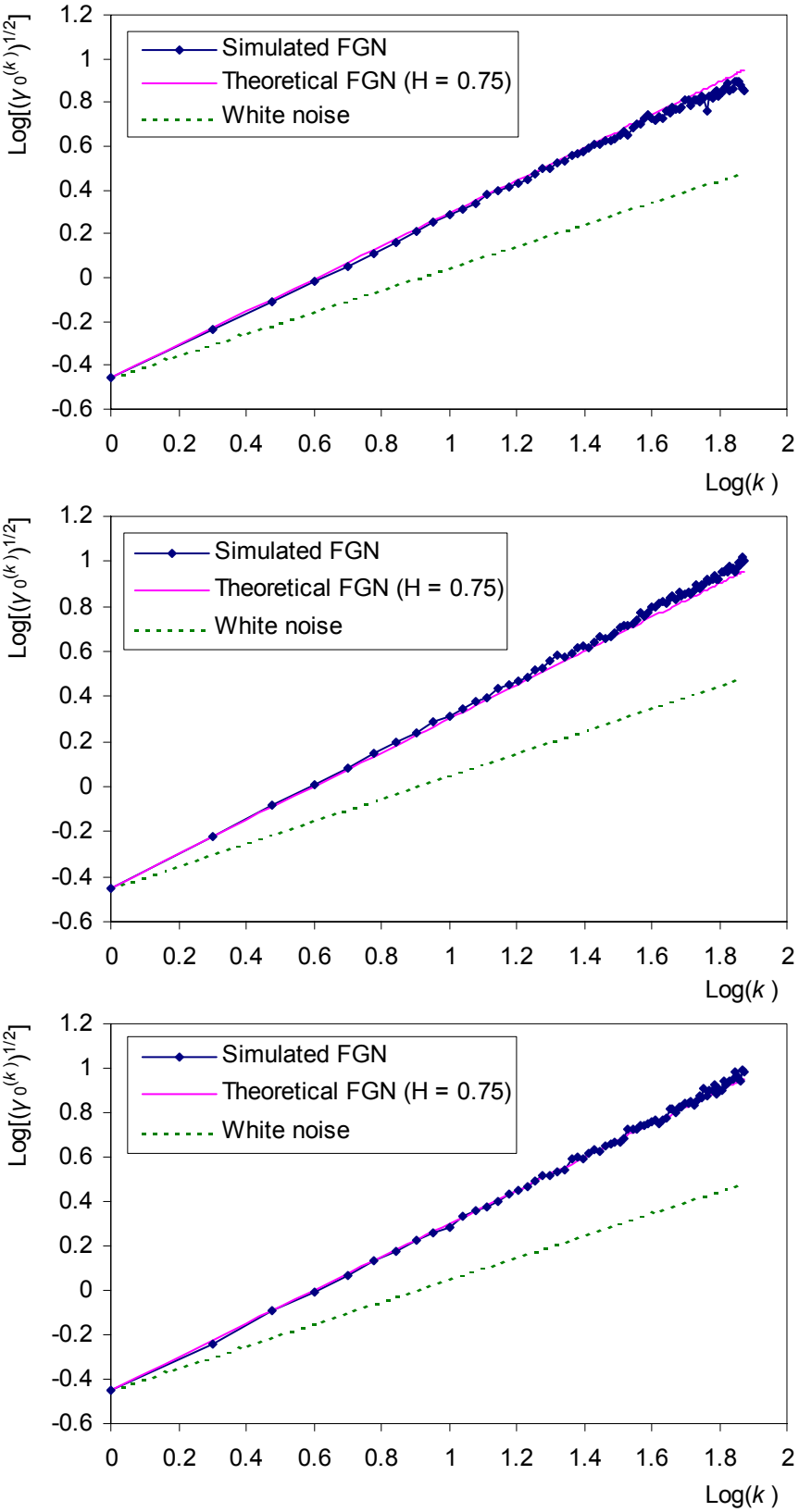

Figure 11 Standard deviation of the aggregated processes $Z_i^{(k)}$ versus timescale k (logarithmic plots) for the three synthetic time series generated using: (up) the multiple timescale fluctuation approach; (middle) the disaggregation approach; (down) the symmetric moving average approach. For comparison we have also plotted the theoretical curves of the white noise and FGN models.

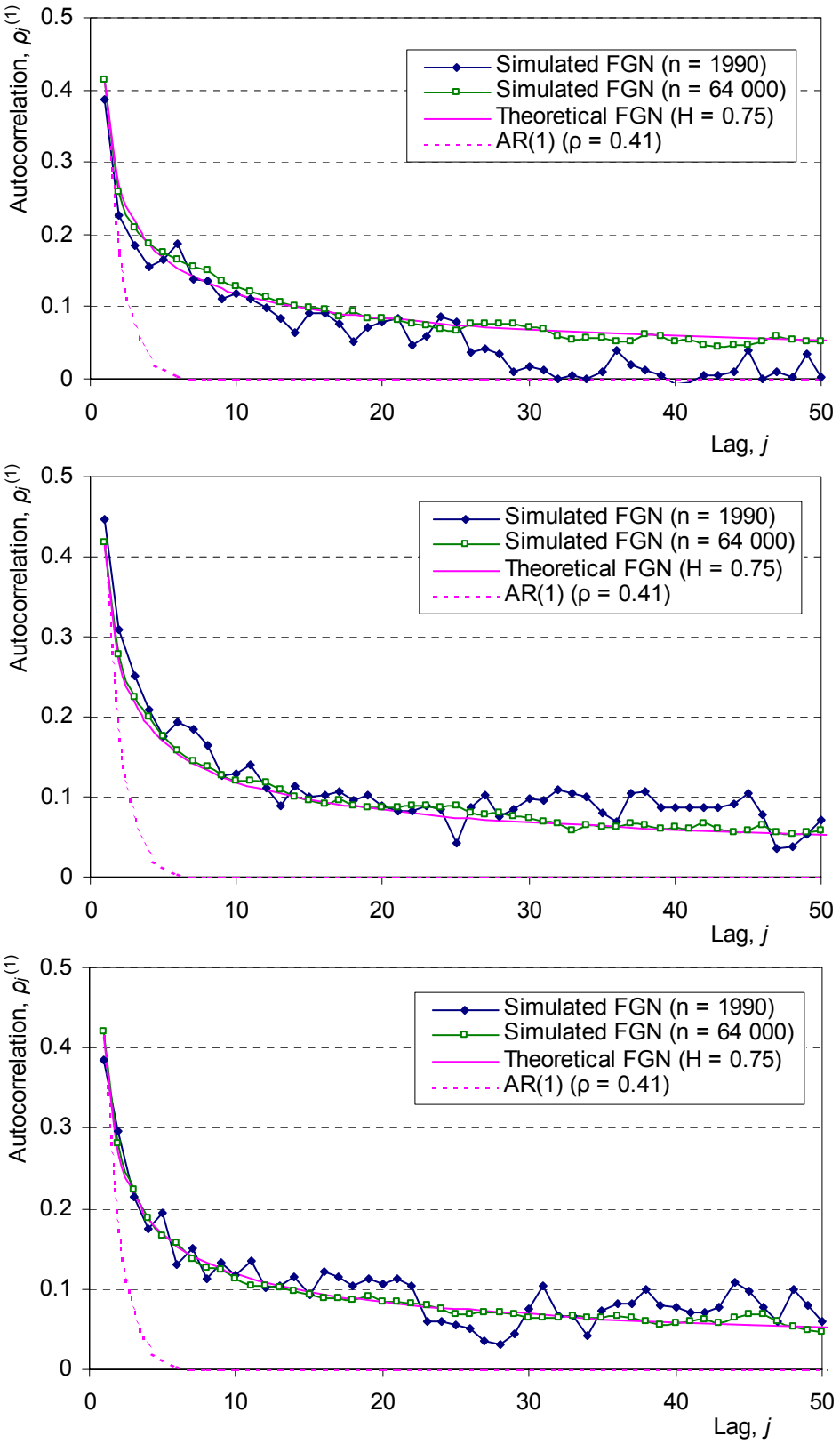

Figure 12 Autocorrelation functions of the three synthetic time series at the basic (annual) scale generated using: (up) the multiple timescale fluctuation approach; (middle) the disaggregation approach; (down) the symmetric moving average approach. For comparison we have also plotted the theoretical curves of the AR(1) and FGN models and empirical functions of three additional series with large length (64 000) generated using the same three methods.

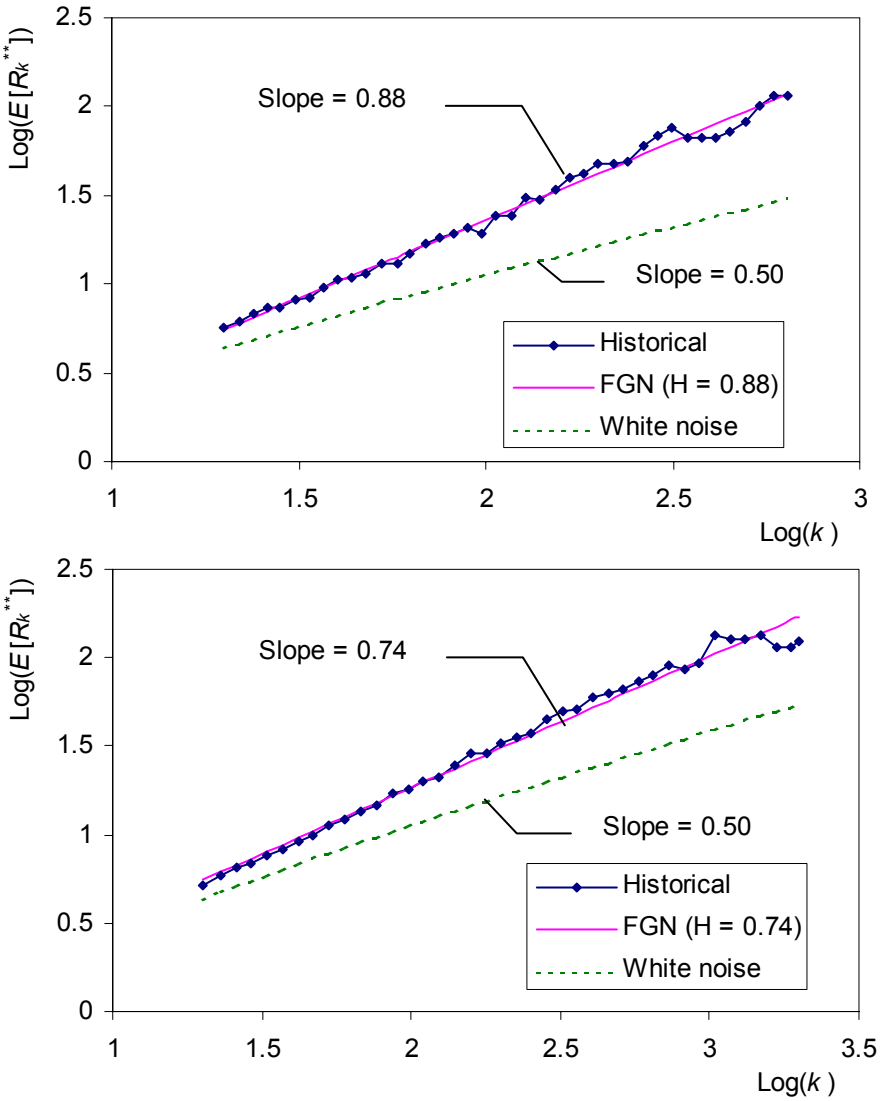

Figure 13 Mean rescaled range $E[R_k^{**}]$ versus time length k (logarithmic plots) for the two example historical data sets: (up) annual minimum water level of Nile; (down) standardised tree rings at Mammoth Creek, Utah. For comparison we have also plotted approximate theoretical curves for the white noise and FGN models.

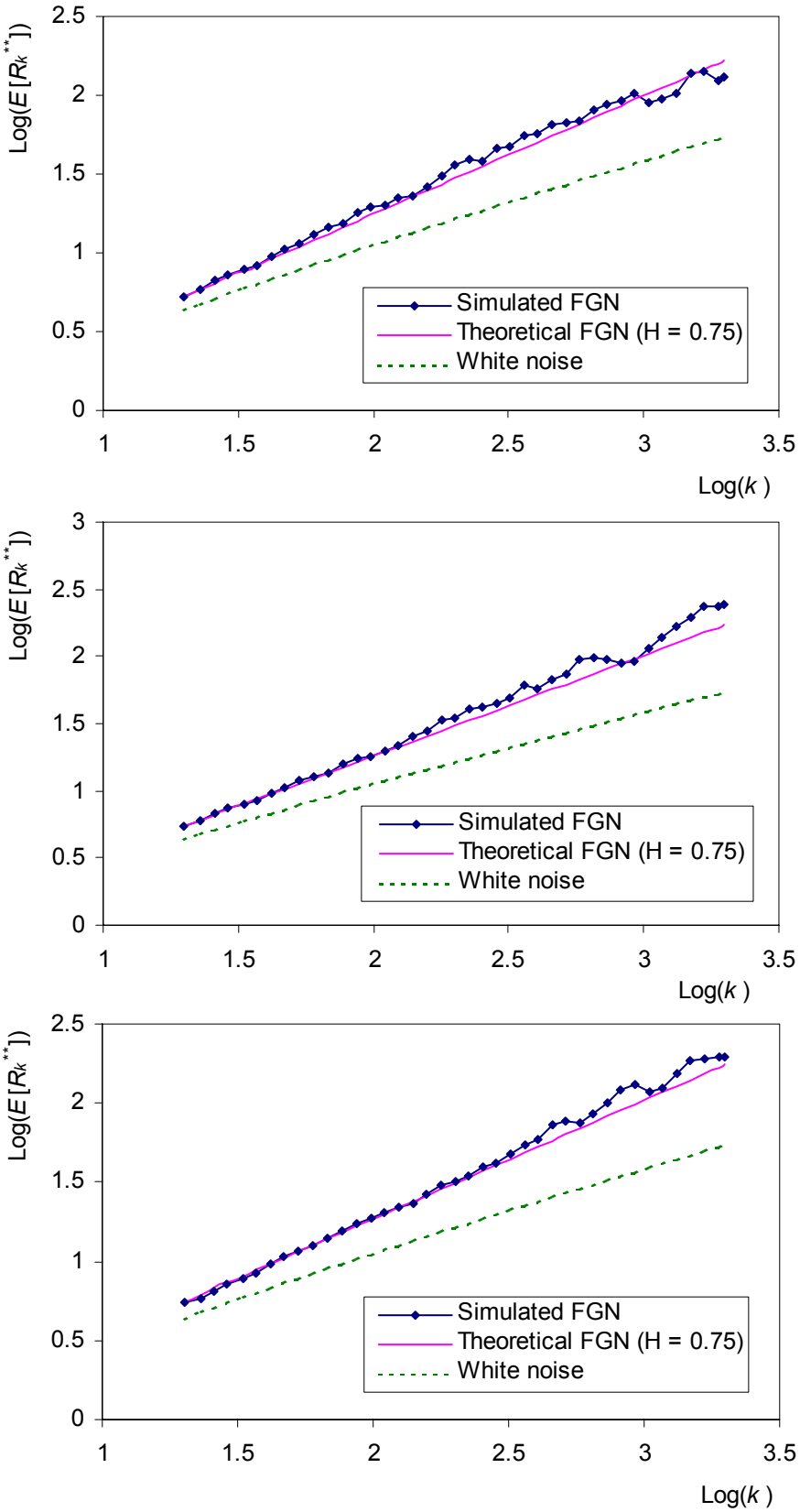

Figure 14 Mean rescaled range $E[R_k^{**}]$ versus time length k (logarithmic plots) for the three synthetic time series generated using: (up) the multiple timescale fluctuation approach; (middle) the disaggregation approach; (down) the symmetric moving average approach. For comparison we have also plotted approximate theoretical curves for the white noise and FGN models.